Glacial-interglacial climate changes recorded by debris flow fan deposits, Owens Valley, California

Mitch D'Arcy[1]*; Duna C. Roda-Boluda[1]; Alexander C. Whittaker[1]

[1]Department of Earth Science and Engineering, Imperial College London, South Kensington Campus, Exhibition Road, London SW7 2AZ, United Kingdom

*Corresponding author. Email: mdarcy@uni-potsdam.de; Phone: +49 331 2882 8832; Present address: University of Potsdam, Institute of Earth and Environmental Science, Karl-Liebknecht-Str. 24-25, 14476 Potsdam-Golm, Germany

Abstract

It is hotly debated whether and how climate changes are recorded by terrestrial stratigraphy. Basin sediments produced by catchment-alluvial fan systems may record past climate over a variety of timescales, and could offer unique information about how climate controls sedimentation. Unfortunately, there are fundamental uncertainties about how climatic variables such as rainfall and temperature translate into sedimentological signals. Here, we examine 35 debris flow fan surfaces in Owens Valley, California, that record deposition throughout the past 125,000 years, during which climate has varied significantly. We show that the last full glacial-interglacial cycle is recorded with high fidelity by the grain size distributions of the debris flow deposits. These flows transported finer sediment during the cooler glacial climate, and became systematically coarser-grained as the climate warmed and dried. We explore the physical mechanisms that might explain this signal, and rule out changes in sediment supply through time. Instead, we propose that grain size records past changes in storm intensity, which is responsible for debris flow initiation in this area and is decoupled from average rainfall rates. This is supported by an exponential Clausius-Clapeyron-style scaling between grain size and temperature, and also reconciles with climate dynamics, the initiation of debris flows, and observations from El Niño events. The fact that these alluvial fans exhibit a strong, sustained sensitivity to orbital climate changes sheds new light on how eroding landscapes and their sedimentary products respond to climatic forcing. Finally, our findings highlight the importance of threshold-controlled events, such as storms and debris flows, in driving erosion and sedimentation at the Earth's surface in response to climate change.

1. Introduction

Constraining the sensitivity of eroding landscapes and their sediment routing systems to climatic forcing is a key challenge (Molnar & England, 1990; Allen, 2008; Champagnac et al., 2012; D'Arcy & Whittaker, 2014). In particular, a major question is whether and in what circumstances sedimentary signals of past climate changes are preserved in terrestrial stratigraphic records with high fidelity (Blum & Törnqvist, 2000; Whittaker, 2012; Armitage et al., 2013; Foreman, 2014). Climate changes during individual glacial-interglacial cycles in particular (over 10^4 to 10^5 year timescales) bring changes in ocean and atmospheric temperatures, precipitation rates and distributions, glacial activity and ecosystems, among other effects; and these changes impact landscape processes. This includes the erosion, transport, and deposition of sediment, meaning climate changes may generate characteristic signals in sedimentary deposits (Burke et al., 1990; Bull, 1991; Paola et al., 1992; Blum & Törnqvist, 2000). For this reason, the sedimentary record is typically presented as an archive of past environmental change on Earth. This assumption has recently been challenged by studies proposing that sediment routing systems could be buffered against high-frequency climate changes (Castelltort & Van Den Driessche, 2003; Allen, 2008; Armitage et al., 2013) and that sediment transport processes might 'shred' signals of external controls (Hallet, 1990; Humphrey & Heller, 1995; Jerolmack & Paola, 2010). Even if landscapes do react to climate changes, major questions remain about how associated signals are transferred into the stratigraphic record, over which timescales, and with what sensitivity.

Quantitative measures of precisely dated stratigraphy are essential for resolving these questions and understanding the effects of climate change on sedimentation. Here, we present a detailed study of mountain catchment-alluvial fan systems in the eastern Sierra Nevada, California, and we examine their sensitivities to known glacial-interglacial past climate changes. We characterise the properties of the climatic signal preserved in these debris flow-dominated fan deposits, and explore its physical origins.

2. Background

2.1. Theory and models

Basin deposits constitute a record of sediment transfer from eroding catchments to depocentres, and therefore contain information about how erosion, transport and deposition have adjusted to tectonic and climatic boundary conditions (Paola, 2000; Duller et al., 2010; Allen, 2008; Whittaker, 2012). Climate is a key boundary condition because the efficiency of weathering, erosion and sediment transfer is determined by climatic variables such as

moisture availability and rainfall (e.g., Dixon et al., 2009; Steffen et al., 2009; McPhillips et al., 2013).

Numerical models have been used to explore many open questions about the environmental controls on basin fill (e.g., Paola et al., 1992; Allen & Densmore, 2000; Armitage et al., 2011; Simpson & Castelltort, 2012; Allen et al., 2013). Coupled mountain catchments and alluvial fans are good landscape systems to work with because they involve a range of sediment transport processes, but are self-contained and relatively simple to conceptualise and compare with natural examples. They also preserve volumetrically-closed records of rapid erosion and sedimentation that can be easily studied in the field. Catchment-fan models have represented climate change as step-changes or cyclicity in average precipitation rates, and they predict characteristic responses in sediment volumes and grain size distribution delivered to alluvial fans, and also fan architecture governed by aggradation and incision (e.g., Densmore et al., 2007; Armitage et al., 2011; Simpson & Castelltort, 2012; Allen et al., 2013). Generally, models predict that an abrupt increase in precipitation rate would increase sediment flux and cause the transient progradation of coarse-grained sediment on an alluvial fan, with a reduced down-system rate of grain size fining that is preserved in stratigraphy (Densmore et al., 2007; Armitage et al., 2011; Allen et al., 2013). In these models, an increase in precipitation of 50-100% (realistic for glacial-interglacial cycles), approximately doubles sediment flux, generating kilometres of fan progradation and a coarse spike in grain size on the order of ≥10 mm (or a ~50% change) through a virtual fan cross-section. Laboratory experiments also indicate that eroding landscapes should be sensitive to specific climate changes, e.g., in precipitation rate (Bonnet & Crave, 2003). Physical models of alluvial fans demonstrate that doubling rainfall rate and sediment flux to the fan causes transient coarsening of grain size in stratigraphy (Rohais et al., 2012), an outcome consistent with numerical models.

Overall, these modelling studies suggest that climate changes could be recorded by some landscapes as diagnostic sediment flux and grain size signals delivered to terrestrial basins. During the past ~1 Ma years, the greatest amplitude climate fluctuations have been associated with glacial-interglacial cycles with a periodicity of ~100 kyr: it remains unclear whether source-to-sink sedimentation is sensitive to such rapid perturbations (e.g., Densmore et al., 2007; Armitage et al., 2013; Simpson & Castelltort, 2012). Further questions concern the extent to which climatic signals might be obscured by 'signal shredding' within sediment routing systems (e.g., Humphrey & Heller, 1995; Clarke et al., 2010; Jerolmack & Paola, 2010). Here, signals may be filtered by thresholds within the sediment transfer pathway (Jerolmack & Paola, 2010), or suffer interference with sediment transport fluctuations arising from self-organised behaviour (Paola & Foufoula-Georgiou, 2001). Models are also limited by

103 necessary process simplifications, and usually do not fully account for factors like the intensity
104 distribution of precipitation, runoff modulators like vegetation cover, or sediment transport by
105 threshold-controlled hillslope processes (e.g., Fernandes & Dietrich, 1997; Tucker &
106 Slingerland, 1997; Istanbulluoglu & Bras, 2006). Consequently, it remains unclear from
107 theoretical work whether we should expect to find records of various climate changes in basin
108 stratigraphy or not. Empirical studies are therefore needed to evaluate landscape sensitivity
109 to known past climate changes.

110

111 ## 2.2. Observations

112 Real sedimentary deposits can be examined to determine whether or not they preserve
113 records of known climate changes in the past. Glacial-interglacial climate cycles offer an
114 important opportunity to study landscape responses to environmental change, involving well-
115 constrained, high-amplitude climate fluctuations over short (10^4 to 10^5 year) timescales during
116 which tectonic conditions are typically constant. As a result, late Pleistocene-Holocene climate
117 changes have been invoked to explain alluvial fan deposits from a range of locations, often
118 correlated with the timings and magnitudes of fan aggradation and incision events (e.g., Bull,
119 1991; McDonald et al., 2003; Steffen et al., 2009; Miller et al., 2010). However, a long-standing
120 debate persists about the processes that construct alluvial fans and whether they record past
121 climate changes (e.g., Blackwelder, 1928; Beaty, 1963; Hooke, 1967; Bull, 1991). Where
122 precise chronologies are available, fan depositional events have been correlated to periods of
123 enhanced precipitation and storm intensity, e.g., in the south-western United States
124 (McDonald et al., 2003; Miller et al., 2010; Antinao & McDonald, 2013a,b; Fuchs et al., 2015)
125 and elsewhere (Steffen et al., 2009, 2010; Bekaddour et al., 2014).

126 In the subtropical Andes, Bookhagen & Strecker (2012) and McPhillips et al. (2013) used ^{10}Be
127 cosmogenic nuclides to infer that catchment erosion rates were significantly higher in the late
128 Pleistocene compared to the Holocene, potentially due to a wetter, stormier climate increasing
129 sediment supply by surpassing erosion thresholds. Also in the Andes, Steffen et al., (2009,
130 2010) and Bekaddour et al. (2014) were able to use stratigraphy, sedimentology and
131 cosmogenic nuclides to link fan aggradation sequences for the last ~100 kyr with wetter
132 periods in the late Pleistocene, followed by incision events when hillslope sediment supplies
133 were exhausted. In the Mojave Desert of California, an arid landscape, Miller et al. (2010)
134 demonstrated that alluvial fans aggraded at times of heavy rainfall associated with enhanced
135 monsoonal activity and warmer sea surface temperatures. Nearby in Baja California, Mexico,
136 Spelz et al. (2008) inferred that fan deposition was promoted by a wetter climate in the past,
137 and that fan terraces can be correlated with Milankovitch cycles during the last ~200 kyr.

Finally, Dühnforth et al. (2007) examined debris flow-dominated fan deposits in Owens Valley in particular, and identified discrete fan surfaces associated with marine isotope stages during the last glacial cycle. These examples imply that catchment-fan systems can be sensitive to glacial-interglacial climate changes in terms of their architecture, sedimentary characteristics and deposition rates. However, some disagreements remain about whether fan aggradation is promoted by wetter climates (Steffen et al., 2009, 2010; Waters et al., 2010; Bekaddour et al., 2014; Owen et al., 2014), stormier climates (McDonald et al., 2003; Miller et al., 2010; Antinao & McDonald, 2013a,b; Fuchs et al., 2015), arid climates and a decrease in vegetation cover (Langbein and Schumm, 1958; Bull, 1991; Pelletier, 2014) or autogenic processes unrelated to climate (Humphrey & Heller, 1995; Paola et al., 2009; Clarke et al., 2010).

Other studies have considered the sedimentological characteristics of the deposits themselves. For example, grain size distributions can be quantified easily, are readily preserved, and are known to record information about sediment supply, sediment transport, and the sensitivity of catchments to tectonic and climatic boundary conditions (e.g., Stock et al., 2007; Whittaker et al., 2007, 2010; Duller et al., 2010; Waters et al., 2010; Foreman et al., 2012; Allen et al., 2013; D'Arcy et al., 2016). D'Arcy et al. (2016) measured rates of grain size fining from apex to toe on channelized fans in Death Valley, California, and interpreted these to record a decline in sediment flux of ~20% as the climate became more arid and precipitation rates declined by ~30%. These results show that useful information can be retrieved from deposit sedimentology, yet sedimentological responses to climate change (e.g., grain size) still remain less well-studied in alluvial fan systems than geomorphological responses (e.g., incision and aggradation) or stratigraphic responses (e.g. progradation and retrogradation) (Densmore et al., 2007; Armitage et al., 2011; Allen et al., 2013).

Here, we test whether the grain size distributions of alluvial fan deposits record a clear signal of glacial-interglacial climate changes. Suitable study areas should meet five key criteria: (1) the sedimentary deposits need to be mapped and dated at a high resolution in time and space; (2) catchment-fan systems need to have experienced high-amplitude, well-documented climate changes in the past; (3) other boundary conditions need to be constant, including tectonics and bedrock lithology; (4) good sediment preservation is important, including the rapid generation of accommodation, frequent abandonment of fan surfaces, and minimal post-depositional reworking; (5) multiple discrete systems should be compared to evaluate the reproducibility of any climate signal observed. We have targeted Owens Valley, California, as an ideal study area meeting these criteria. We measure grain size distributions on 35 dated fan surfaces, and show how they vary over the past 125 kyr in comparison with regional palaeoclimate records. We then explore potential explanations for the climate sensitivity

observed, involving past glaciation, sediment sources, weathering of bedrock, and changes in the mobility and transport of sediment by debris flows.

3. Study Area

3.1. Geomorphological and geological setting

We examined 8 individual mountain catchment-alluvial fan systems along the eastern front of the Sierra Nevada range in California, located near the towns of Independence and Big Pine (Fig. 1). From north to south, these are the Birch, Independence, Pinyon, Symmes, Shepherd, North Bairs, South Bairs, and George Creek systems. They drain eastward into Owens Valley constructing a coalesced bajada of large alluvial fans ~10 km long and with surface gradients of 4 to 6°. These basin deposits have a total thickness of around 2.4 km (Pakiser et al., 1964), and are not toe-cut by the axial Owens River or ancient lake shorelines at this location. The fans occupy an elevation of 1500 to 2000 m above sea level, with the catchments rising to the Sierra Nevada crest line at approximately 4000 m, eroding ~2000 m of total relief (Fig. 2a). Catchment areas range from 8.0 km^2 (south Bairs Creek) to 33.9 km^2 (Shepherd Creek). All catchments erode almost exclusively granitic bedrock—comprising Mesozoic granodiorites and quartz monzonites of a number of plutons, particularly the Bullfrog, Dragon, and Paradise granites—with very minor outcrops of metavolcanic rocks (Moore, 1981; Moore & Sisson, 1987). The alluvial fan sediments are therefore granitic in composition, and have been mapped and dated in great detail by a number of previous studies (Zehfuss et al., 2001; Dühnforth et al., 2007; Le et al., 2007; D'Arcy et al., 2015). Catchment hillslopes are steep (characterised later) and vegetation cover is sparse, with low-density pine and juniper woodland at middle elevations transitioning to desert scrub on the alluvial fans. Representative field photographs are shown in Fig. 3. Sediment is supplied by widespread landsliding and steep scree cones, weathering of exposed bedrock faces, and incision into glacial moraine deposits. The catchments are dominated by hillslope processes, connected to the main channels, and as a result their fans have been almost entirely constructed by debris flows (Bierman et al., 1991; Whipple and Dunne, 1992; Dühnforth et al., 2007; Le et al., 2007).

The catchments are separated from the fans by the southern section of the Sierra Nevada Frontal Fault Zone (SNFFZ), an active normal fault system generating a steep, range-bounding escarpment striking north-north-west (Fig. 1). The SNFFZ was likely active from the late Miocene onwards, and involved in the break-up of a pre-existing plateau (Phillips, 2008; Jayko, 2009). The slip rate accelerated during the Plio-Pleistocene, attributed to lithospheric delamination, but the current tectonic regime has been stable for >1 Ma (Wakabayashi &

Sawyer, 2001; Jones et al., 2004; Stock et al., 2004; Clark et al., 2005; Jayko, 2009). Good constraints are available for the displacement history of the frontal normal fault system for at least the last 300 kyr (Gillespie, 1982; Martel et al., 1987; Zehfuss et al., 2001; Le et al., 2007). Dated fault scarps give vertical displacement rates of 0.2 to 0.3 mm yr^{-1} on parallel fault strands (Zehfuss et al., 2001; Le et al., 2007), summing to a total displacement rate of ~1 mm yr^{-1} between the catchments and the valley. Scarp measurements also reveal that displacement rate on the SNFFZ has been steady for at least 300 ka, with no changes in tectonic activity during the last glacial-interglacial cycle (Martel et al., 1987; Zehfuss et al., 2001; Le et al., 2007). Therefore, these catchment-fan systems have experienced constant lithological and tectonic boundary conditions during the pronounced climate changes of the last glacial-interglacial cycle, allowing the climatic control on sedimentation to be isolated.

3.2. Modern and past climate

The catchments along the eastern escarpment of the Sierra Nevada occupy a rain shadow, as the majority of precipitation originates from Pacific sources to the west (Fig. 4). Moisture sources include extra-tropical cyclones, which occur during the winter months and last a day or longer with precipitation intensities of 5-7 mm/hr; these mid-latitude storm paths are guided by the polar jet stream and typically intensify during El Niño (Antinao & McDonald, 2013a). Additionally, atmospheric rivers carry storms along narrow jets from the tropical Pacific, and can generate rainfall intensities of >10 mm/hr lasting a day or more. These storms occur throughout the year, and are more intense when sea surface temperatures are warmer off the coast of California (Persson et al., 2005). The remnants of tropical cyclones affect the southwestern United States during late summer and autumn, and on average produce rainfall intensities of about 5 mm/hr lasting 48 hours, although the most extreme hurricanes have produced 10 mm/hr lasting for 24 hours (cf. Antinao & McDonald, 2013a). Finally, the North American Monsoon delivers moisture from the eastern Pacific, Gulf of California, and Gulf of Mexico during the summer and early autumn. The monsoon typically produces isolated thunderstorms with rainfall intensities <10 mm/hr lasting a few hours, and heavy thunderstorms can trigger severe runoff and debris flows (DeGraff et al., 2011). Known thresholds for debris flow initiation are surpassed by rainfall intensities of 5-10 mm hr^{-1} for a duration of 1-2 hours, and with greater rainfall intensities only short downbursts are required to trigger a debris flow (Cannon et al., 2008; Coe et al., 2008).

In this study area, mean annual precipitation is 800-900 mm yr^{-1} at the top of the catchments and decreases abruptly towards the east (Fig. 4b) (PRISM climate group, 2004; Kessler et al., 2006). Average annual temperatures are as low as 0°C at the Sierra Nevada crest. At the fan

242 toes in Owens Valley, average annual precipitation is 50-200 mm yr^{-1} depending on the year,
243 and mean annual temperature is 14-18 °C (NOAA National Climatic Data Center, 2014). In
244 summary, the study catchments experience a relatively dry climate today, with orographic
245 gradients in precipitation rate and temperature, and a substantial rainfall contribution from
246 storms that originate in various parts of the Pacific.

247 In the south-west USA, the climate during the last glacial period was significantly cooler and
248 wetter than today. Evidence for this includes dated lake shorelines (Orme & Orme, 2008) and
249 cores (Benson et al., 1996), vegetation records (Woolfenden, 2003), glacial moraines and
250 landforms (Phillips et al., 2009; Rood et al., 2011), and terrestrial oxygen isotope records
251 (Winograd et al., 1997, 2006), among other data (Phillips, 2008, provides a review). Parts of
252 our study catchments were occupied by valley glaciers during the coolest parts of the last
253 glacial-interglacial cycle, which have since retreated (Brocklehurst et al., 2008; Duhnforth et
254 al., 2008; Moore & Mack, 2008). Glaciation has produced stepped longitudinal profiles (Fig.
255 2a), U-shaped troughs in parts of the catchments (Fig. 3b), and glacial landforms. Time series
256 of glacial rock flour deposition in Owens Lake cores have also been described (e.g., Bischoff
257 et al., 1997). The maximum extent of glaciation varies significantly between the catchments
258 (Fig. 1). Some, e.g., Birch Creek and Independence Creek were fully occupied at the peak of
259 glaciation. However others, e.g., Shepherd Creek, Pinyon Creek, and the Bairs Creek
260 catchments, were only ever partly glaciated and have valleys unaffected by glaciation in their
261 lower reaches.

262 Several different methods have been used to estimate how much cooler and wetter the Last
263 Glacial Maximum (LGM) was compared to today. Pollen data from packrat middens in western
264 Nevada, at the same latitude as our study catchments, indicate the LGM was 5-8°C cooler
265 and 2.2-2.4 times wetter than today (Thompson et al., 1999). Similarly, oxygen isotope data
266 from ostracod fossils in southern Nevada suggests the LGM was at least 5.6°C cooler (Quade
267 et al., 2003), and hydrological restorations of pluvial lakes model the LGM as ~5°C cooler and
268 1.5-2.0 times wetter than present (e.g., Menking et al., 2004). Sensitive numerical models of
269 mountain glaciers in the southern Sierra Nevada require a temperature depression of 5.6°C
270 and a factor of 1.9 increase in total precipitation in order to simulate the correct spatial extents
271 known from mapped LGM glacial landforms (Kessler et al., 2006). Therefore, the LGM climate
272 is constrained at 5 to 6°C cooler and twice as wet (on average) than modern conditions, and
273 this represents the amplitude of glacial-interglacial climate changes in this area. Why was the
274 late-glacial climate wetter in the SW United States? Often, this is attributed to a southward
275 shift of mid-latitude westerly storms resulting from the presence of the Cordilleran and
276 Laurentide ice sheets, which may have split and deflected the polar jet stream (COHMAP
277 members, 1988; Oster et al., 2015). However, enhanced moisture transport from the tropical

Pacific may also have contributed to wetter conditions in the SW USA at the LGM (Lyle et al., 2012; Kirby et al., 2012).

Several continuous regional palaeoclimate records are also available. The Devil's Hole $\delta^{18}O$ record is a high-resolution terrestrial oxygen isotope curve from calcite veins in southern Nevada, close to our study area (Winograd et al., 1997, 2006). Its chronology, based on $^{230}Th/^{234}U$ series dating, captures 10^3 to 10^5 year climate fluctuations (Fig. 5b), and is highly correlated with past sea surface temperatures (Winograd et al., 2006). Also, a number of alkenone-derived sea surface temperature reconstructions have been reported along the Californian coast (c.f., Lyle et al., 2010), of which the ODP-1016 record in the Santa Barbara basin (Yamamoto et al., 2007) is the closest to our study area (Fig. 5c). This shows modern temperatures of ~16°C decreasing to ~12°C at the LGM, having gradually cooled from a peak of ~18°C during the last interglacial (Fig. 5). This record is highly correlated with equivalent sea surface temperature records from nearby locations (Lyle et al., 2010), although the absolute temperatures naturally vary with latitude.

The timings of climate changes within the last glacial cycle are equally important for our analyses as their amplitudes. Exposure dating of LGM (Tioga) moraines shows that mountain glaciers advanced to their peak extents at ~26 ka, and retreated rapidly at 21 to 17 ka along the entire eastern margin of the Sierra Nevada (Phillips et al., 2009; Rood et al., 2011). In Owens Lake cores, *Juniperus* and other tree pollen dominate from 26 to 18 ka, before declining from 18 to 10 ka as the drying climate allowed desert scrub to dominate (Woolfenden, 2003). *Juniperus* abundance in particular is highly correlated with orbital climate shifts captured by $\delta^{18}O$ records (Woolfenden, 2003) and is shown in Fig. 5d. Organic and inorganic carbon input into Owens Lake also decreased abruptly between 26 and 20 ka (Benson et al., 1996), and dessication events in the lake have been identified from 18.3 ka onwards (Benson et al., 1996). The penultimate (Tahoe) glaciation was longer in duration and more extreme, with moraines extending further down the catchments and their ^{36}Cl exposure ages indicating retreat around 135 kyr ago (Phillips et al., 2009), in agreement with global timings (e.g., Lisiecki & Raymo, 2009). Temperatures may also have been ~10 °C lower than modern averages (Quade et al., 2003). This was followed by a rapid decrease in *Juniperus* pollen in Owens Lake cores between 126-130 ka (Woolfenden, 2003), and a rise in temperature indicated by the Devil's Hole $\delta^{18}O$ curve, placing the local last interglacial at 120 to 130 ka (Winograd et al., 2006).

3.3. Debris flow-dominated fan deposits

The eight catchment-fan systems studied here (Fig. 1) are dominated by debris flows (Dühnforth et al., 2007; Le et al., 2007; D'Arcy et al., 2015), with only minor reworking by streams and small superficial sheet-floods. Many studies have shown that debris flows can be generated by surface runoff (e.g., Coe et al., 1997; Cannon et al., 2008; Kean et al., 2011, 2013; Hobley et al., 2012; Staley et al., 2014; Rengers et al., 2016), including in this study area (DeGraff et al., 2011). As such, debris flows are highly sensitive to triggering storms when sediment supply is abundant and non-limiting (Kean et al., 2011, 2013). Individual debris flows in the Sierra Nevada can move >1.5 million m^3 of material in the most extreme cases and flow with velocities between 2-8 m s^{-1} (DeGraff et al., 2011).

The sediment transport mechanics of debris flows are not fully understood and are considerably more complex than for streams (e.g., Iverson et al., 2010). Nonetheless, the sedimentology of debris flow deposits contains useful information about properties such as event size and discharge (McCoy et al., 2013). For example, the grain size distribution carried by some debris flows in the USA has been shown to be coarser in larger flows (Coe et al., 2008; McCoy et al., 2012, 2013), indicating empirically that more powerful flows may transport coarser material, even if the underlying equations remain unknown. One key characteristic is the segregation of larger particles to the tops, sides, and fronts of flows, resulting from internal fluid pressure gradients and buoyancy forces (Johnson et al., 2012). Debris flow deposits therefore have distinct gravel channels bound by coarse, boulder-rich lateral levees exhibiting upward-coarsening (Fig. 3e). These properties are obvious on the alluvial fan surfaces in Owens Valley, which comprise a network of abandoned and cross-cutting debris flow channels and levees carrying boulders typically 0.5 to 3.0 m in diameter, but sometimes 10 m or larger. Individual flow deposits are 10s of metres wide, measured from levee to levee, and sometimes inherit pre-existing flow pathways (Fig. 3d, f). Due to the clear channel and levee segregation, depositional relief and inverse grading in these deposits, we interpret them to represent typical debris flows (Whipple & Dunne, 1992).

Debris flows rapidly transfer sediment from catchment sources to fans, and may therefore also rapidly transmit signals of environmental forcing, e.g., climate, to basin deposits. They form thick aggraded surfaces on the Owens Valley fans (Fig. 3c) that are well-preserved. A total of 35 fan surfaces, distributed across the 8 fans, have been mapped and dated by previous workers using (i) ^{10}Be cosmogenic nuclide exposure dating (Zehfuss et al., 2001; Dühnforth et al., 2007; Le et al., 2007), and (ii) weathering fractures in surface boulders whose dimensions can be precisely calibrated as age indicators using the ^{10}Be chronology (D'Arcy et al., 2015). The stratigraphy for these systems is summarised in Fig. 5a. Each dated surface

contains deposits from many debris flow events of similar age, and the various units are clearly exposed around the fan apices, dissected by younger surfaces that incise into older deposits (Dühnforth et al., 2008; D'Arcy et al., 2015; Fig. 3c). All of the fans show past incisional events (Fig. 5a), but the timings of incision vary from fan to fan. Modern, active debris flow channels on all 8 fans are now incising into older deposits, including Holocene sediments. Other than the timing of ancient incision events, few differences exist between the fans. Their debris flow deposits are comparable in terms of sedimentological properties and overall sizes, and the fans share the same depositional lengths, granitic source lithology, and tectonic setting. As a result of incision and avulsion, older surfaces quickly become inactive and are abandoned within 10-20 kyr (D'Arcy et al., 2015; Fig. 5a).

4. Methods

4.1. Sampling

As grain size is a fundamental characteristic of sedimentary deposits, we measured grain size distributions across debris flow fan surfaces, in order to test whether these data record sensitivity to past climate fluctuations. Debris flow deposits were sampled on 35 fan surfaces, distributed across 8 catchment-fan systems in Owens Valley. These deposits have been mapped and dated in detail by previous workers using ^{10}Be cosmogenic nuclides and correlation techniques (Zehfuss et al., 2001; Dühnforth et al., 2007; Le et al., 2007; D'Arcy et al., 2015).

Grain size was measured in the field by Wolman point counting (Wolman, 1954) at 292 different sampling localities. Localities were chosen where the fan deposits exhibit clear characteristics of debris flow deposition (inverse grain size grading and a clear segregation of material into channels and levees; see section 3.3).. At each surface locality (see supplementary information for locations), the long-axis diameters of a minimum of 100 randomly-selected clasts above 1 mm in size were recorded. Separate counts were made for debris flow channels (15,737 clasts in total) and lateral levees (14,878 clasts). We did not sample finer particles as their mobility is likely to be high and fines have been documented in detail from cores through the Owens Lake sediments, which represent the end of the depositional system and are more suitable for characterising the very fine fraction (Benson et al., 1996; Menking, 1997). Our grain size data therefore describe the gravel fraction that is well-preserved on the fans and not affected by aeolian modification. Grain size was sampled from deposits on the debris flow fan surfaces, but where sub-surface sections were visible (e.g., incised sections) we detected no differences in the gravel grain size distribution

compared to surfaces We characterised the fining rate from apex to toe on the Q4 (Holocene) surface of the Shepherd Creek fan (Fig. 6) to constrain any effects arising from down-system fining. For all other fan surfaces we restricted our grain size sampling to the upper 3 km of the alluvial fans, to avoid potential fining effects, and also because many older surfaces are only exposed near the fan apices (Fig. 1). On each dated fan surface, an average of 8 different localities (a minimum of 3 and a maximum of 12) were sampled. This ensures that the overall grain size distributions are spatially representative.

Our analysis relies on the assumption that the gravel grain size distribution is not significantly altered by post-depositional processes. In our Wolman point counts, we avoided clasts that were obvious weathering products, e.g., thin sheets of granite that had been exfoliated from boulders by superficial weathering. We selected localities on stable parts of older surfaces, away from younger flow events, and desert pavement formation is minor in Owens Valley. While we document no correlation between deposit age and grain size fining, our data offer the opportunity to evaluate the importance of any post-deposition effects, which we revisit in section 6.

Sediment sources were also sampled in two catchments, to provide a comparison with the fans: Independence Creek, which is larger (25.6 km^2) and was fully glaciated at the LGM, and Symmes Creek, which is smaller (11.8 km^2) and was partially glaciated (Fig. 1). We again used Wolman point counting to measure the surface grain size distributions of hillslope landslides (3 sites), steep scree cones (4 sites), and glacial moraine deposits (11 sites) in each catchment, using identical methods to the debris flow fan deposits described above. These represent the major sediment sources in this area. The locations of moraine deposits in Fig. 1 follow the map of Moore and Mack (2008), but were refined in the field and using high-resolution aerial imagery. Slope distributions for the parent catchments were derived from the National Elevation Dataset (NED) digital elevation model, which has horizontal and vertical spatial resolutions of 9.0 and 1.5 m, respectively, in this area (Gesch et al., 2002). All data are provided in the supporting information.

4.2. Data analyses

For each dated fan surface, the Wolman point counts from every locality were compiled into a single cumulative grain size distribution curve. In order to convert the grain size data into time series, we extracted the median (D_{50}) and 84th percentile (D_{84}) particle diameters from each distribution curve. We assign uncertainties to the surface-averaged D_{50} and D_{84} values equal to ±1 standard deviation among all sampled localities per fan surface (representing the spatial variability in these grain size percentiles on each surface). In other words, if each grain size

415 percentile is calculated at every sampling location on a single fan surface, there will be some
416 variability in the values of D_{50} and D_{84} measured. We use this spatial variability to place
417 uncertainties on the grain size percentiles calculated for each fan surface as a whole.

418 We also repeated the same analyses on the data, but binned across all 8 alluvial fan systems,
419 i.e., grain size data from all Q4 localities were assembled into a single cumulative distribution
420 curve representing all Q4 units across all fans, and likewise for each other unit. We describe
421 these data as 'stratigraphic averages', and assign them the mean ages for each unit. This
422 smoothing technique reduces the temporal resolution of the data set, but increases the size
423 of the data populations to produce D_{50} and D_{84} measurements that represent the full local
424 landscape response by binning and stacking the 8 systems and increasing the signal/noise
425 ratio. These stratigraphic averages are plotted on all graphs using star symbols to distinguish
426 them from individual fan surface data. Again, uncertainties on the stratigraphic average D_{50}
427 and D_{84} are calculated by measuring these grain size percentiles at each individual sampling
428 site, and taking ±1 standard deviation of these values.

429 The grain size percentiles of the 35 dated fan surfaces, plus stratigraphic averages, can be
430 treated as time series and compared with palaeoclimate records. For this purpose we favoured
431 the benthic Pacific $\delta^{18}O$ stack of Lisiecki and Raymo (2009) (Fig. 5b) as a general record of
432 the last glacial-interglacial cycle with a high signal/noise ratio, and the ODP-1016 sea surface
433 temperature reconstruction of Yamamoto et al. (2007) as a regional record of temperature
434 located just offshore California, close to our study area.

435 The alluvial fan surface ages are based on those recompiled and recalculated by D'Arcy et al.
436 (2015) using the ^{10}Be measurements from previous studies (Zehfuss et al., 2001; Le et al.,
437 2007; Dühnforth et al., 2007), and readers are directed to this publication for a full account of
438 the fan surface dating. Typically, the age uncertainties are less than ~10 kyr for surfaces
439 younger than 50 kyr, and 10-20 kyr for older deposits up to Q1 on Birch Creek, which is the
440 oldest surface, and this range includes the timespan over which each surface was active.
441 However, because the the Q1 surface on the Birch Creek fan must date to the last interglacial
442 period we pin this surface at 122.5 ka and adjust the chronology of D'Arcy et al. (2015)
443 accordingly (see supporting information). The uncertainties on fan surface ages remain
444 unchanged and are described by D'Arcy et al. (2015). A full account of the fan surface age
445 constraints is included in the supplementary material. Data were analysed using OriginPro
446 v.9.1 and ArcGIS v.10.3.

447

5. Results

5.1. Down-fan rates of grain size fining

Figure 6 shows the D_{50} grain size (a) and the D_{84} grain size (b), along the full ~10 km length of the Q4 (Holocene) surface of the Shepherd Creek fan, for both debris flow channels (solid black) and their lateral levees (open red). In general, the grain size fining rates are low compared to the actual grain sizes measured, which we attribute to the physical properties of the debris flows in this area. The D_{50} decreases by 0.9 ±0.2 mm km^{-1}, from an initial input grain size of 25 ±1 mm in the channel, while D_{84} simultaneously decreases by 2.1 ±0.4 mm km^{-1}, from an initial grain size of 39 ±2.0 mm. These values represent 3.5-5.0% of the initial grain size, respectively. Similarly, D_{50} data from levee deposits show negligible downstream fining over the 10 km fan length; D_{84} decreases by 7.1 ±1.1 mm km^{-1} from an input value of 111 ±5.0 mm, a fining rate which is 6% of the initial grain size. The low down-system fining rates indicate that small differences in distance from fan apex to measurement site are indeed unlikely to significantly affect grain size measurements for debris flow deposits in this study. Furthermore, all our subsequent sampling localities lie within the upper 3 km of the fans (blue box), except on the Birch Creek fan, where older surfaces are exposed at the base of the fan (see Zehfuss et al., 2001; D'Arcy et al., 2015). Therefore, grain size data from the Birch Creek surfaces may be slightly finer in comparison to the other systems, and we consider the importance of this later.

The down-fan fining effect is smaller than the spatial variability in grain size between individual sampling sites on the same dated fan surface. On average, grain size varies by 20-25% of the median between sampling sites on a given surface, which is to be expected because surfaces comprise deposits from multiple flows that are themselves spatially variable. This underscores the importance of spatial averaging, and making repeat measurements on each dated surface to converge on a grain size distribution that is representative for that surface overall (see Methods). In our subsequent analyses, D_{50} and D_{84} values are extracted from the cumulative grain size distributions that include all localities measured on each surface. Error bars show the standard deviation of D_{50} and D_{84} if they are calculated separately for each sampling site, and therefore display the spatial grain size variability per surface.

5.2. Grain size measurements

In Fig. 7 we show cumulative grain size distribution curves for each stratigraphic unit as a whole (panel a, combining all fan systems), and for every dated fan surface separately (b to i). These are coloured by stratigraphic unit, with warm colours corresponding to surfaces

deposited under interglacial climatic conditions (Q1, Q4, modern), and cool colours corresponding to surfaces deposited under glacial climatic conditions (Q2, Q3). Each cumulative grain size distribution has a sigmoid form with the majority of clasts 10-100 mm in diameter. Levees are ~30 % coarser than channels deposits on average, which is partly due to grain size segregation (e.g., Johnson et al., 2012), and we do not identify any uni-directional changes in this percentage of segregation over time. In all examples, the 'glacial' surfaces (cool colours) are finer-grained than the 'interglacial' surfaces (warm colours), by 10s of mm. The last interglacial (Q1, yellow) data are highly comparable to the current interglacial data (Q4, red, and Modern, pink), and always coarser than Q2 and Q3 surfaces. All 8 fans show similar grain size distributions in terms of percentiles and the differences between surfaces, so it is meaningful to combine these data into composite curves for each stratigraphic unit (panel a). These illustrate clearly how the Q1, Q4 and modern deposits are significantly coarser-grained than the Q2 and Q3 deposits.

These curves can be converted into time series by extracting the D_{50} and D_{84} percentiles (Tables 1 and 2). These are plotted against surface age in Fig. 8, and compared with the benthic Pacific $\delta^{18}O$ stack of Lisiecki and Raymo (2009) as an illustration of climate during the past ~125 kyr (blue curve). In all four percentile series, grain size is significantly coarser in warmer interglacial periods and finer in cooler glacial periods, typically doubling as the climate warmed and dried from the LGM to present. Grain size is coarser in lateral levees than flow channels, as expected. There is a strong and sustained correlation between grain size and past climate, which is equally apparent in other percentiles of the grain size distributions. The D_{50} reaches a minimum of ~15 mm (channels) and ~20 mm (levees) during the glacial period and increases to 25-30 mm during the current and last interglacials. The D_{84} increases from ~30 mm (channels) and ~50 mm (levees) in the glacial period to around 60-80 mm (channels) and 70-90 mm (levees) in the interglacial periods. The rate of fining as the climate cooled after the last interglacial is slower than the rate of coarsening after the LGM, mirroring the asymmetry of the glacial-interglacial cycle. The response timescale is also much shorter than the periodicity of one glacial-interglacial cycle; effectively as short as the temporal resolution of our data (or shorter). We also note that while D_{50} and D_{84} are both calculated from the same grain size distributions, the channel and levee data sets represent independent grain size counts yet both show strong correlations with palaeoclimate. Furthermore, the absolute grain size values and the amplitude of variability through time is the same (within uncertainty) on all 8 fan systems; therefore we do not discriminate between the fans in Fig. 8. The signal amplitude is also larger than the grain size variability on a given fan surface (*y* error bars).

As the data from Birch Creek were collected further down the length of the fan than for the other systems, these points may be slightly finer-grained than for the other fans. Figure 6

indicates that this effect is likely to be very small, at most resulting in a 2-5 mm difference for D_{50} for example. Therefore we do not attempt to apply a correction for this, which would make no material difference to Fig. 8.

Inset panels in Fig. 8 show the grain size series plotted directly against the benthic Pacific $\delta^{18}O$ stack (Lisiecki and Raymo, 2009). Fan surfaces are coloured by age, from dark blue at the last interglacial to green, yellow and orange in the glacial period, and red in the Holocene. These show positive correlations between grain size and lower $\delta^{18}O$ values (warmer climate, reduced continental ice cover), and there is no evidence for hysteresis or directionality in the grain size sensitivity to climate. Stratigraphic averages are plotted as black stars and are fitted with power laws (which represent the data better than other regressions, R^2 around 0.8-0.9), because these points have the greatest signal/noise ratio. These regressions generally show that grain size is related to $\delta^{18}O$ by an exponent of 2-3, i.e., this is a non-linear signal and the sensitivity of grain size to climate increases with warming. The exponents are similar between channels and levees, but slightly variable between D_{50} and D_{84}.

5.3. Sediment sources

Sediment sources in the Sierra Nevada catchments could exert a control on the grain size distribution delivered to fans, so it is important to characterise them. Frequency distributions of surface slope (Fig. 9a) show similar patterns in all catchments, with most slopes between 20° and 50° and significant proportions of hillslopes exceeding ~30°. Sediment supply is therefore largely from hillslope processes and extensive landsliding (Fig. 3a-b). Slopes are slightly lower on average in the most heavily glaciated catchments (Birch Creek and Independence Creek), and formerly-glaciated stepped troughs and cirques are clearly visible as zones of low slope in Fig. 9b. However these glacial troughs are also surrounded by some of the steepest slopes in this landscape, especially in the upper catchments where they can exceed 60°.

The main sediment sources in the catchments are (i) steep and coarse-grained scree cones shed from steep bedrock faces and confined to valley edges; (ii) hillslope landslides that can propagate directly into active channels; (iii) unsorted moraines left behind by past glaciers that have now retreated; and (iv) a minor contribution from direct scouring of bedrock. Each of these sediment sources are sampled by debris flows, and representative photographs are shown in Fig. 10. We sampled each major sediment source in the Independence Creek and Symmes Creek catchments and their cumulative grain size distributions are shown in Fig. 11a. The catchments are not discriminated because the grain size distributions are similar for each sediment source, despite the limited number of sampling sites, which we attribute to the

553 uniform lithology and other boundary conditions across this study area (see section 3). Scree
554 cones are shown in black and are an order of magnitude coarser than landslides (red) and
555 moraines (light blue). Scree cones mostly supply large granite blocks whose sizes are
556 predetermined by joint spacing (Fig. 10b). Moraines provide an intermediate grain size source,
557 with D_{50} ~40 ±5.1 mm and D_{84} between 100 ±26.4 mm and 113 ±6.0 mm, while landslides are
558 finer with D_{50} between 30.5 and 33.0 mm and D_{84} around 82 ±18.3 mm. For comparison, grain
559 size distributions of channels and levees are shown for the modern (yellow) and Q2c (dark
560 blue) units in Fig. 7a, as these represent the coarsest (interglacial) and finest (glacial) end-
561 members from the fans. Apart from the scree cones, the fan deposits are only slightly finer-
562 grained than the sediment sources.

563 As an alternative way of comparing the sediment sources and fan deposits, we have shown
564 the D_{50} values in Fig. 11b. The stars show the stratigraphic averages from Fig. 8, and the
565 coloured boxes show D_{50} ±1 standard deviation for moraines (blue) and landslides (red) as
566 sampled in the Independence and Symmes Creek catchments. These are also quoted in Table
567 3. On average moraines are 5-15 mm coarser than landslides and this difference is similar to
568 the overall amplitude of the climate signal recorded in grain size.

569

570 # 6. Discussion

571 ## 6.1. The nature of the climate signal preserved

572 These debris flow fan systems along the eastern front of the Sierra Nevada, California,
573 preserve in their grain size distributions a striking record of climate changes during the last
574 glacial-interglacial cycle. The flow deposits are significantly coarser-grained during the warm
575 and dry climates of the current and previous interglacials, and finer-grained during the cooler
576 and wetter glacial period. The amplitude of the signal is large (10s of mm), and a 5-6°C
577 warming and an approximate halving of average rainfall rates has led to a doubling of grain
578 size since the LGM, with D_{50} increasing from ~15 mm to ~30 mm. The signal may be non-
579 linear (inset panels of Fig. 8), increasing in sensitivity with warming of the climate.
580 Fundamentally, our results show that these fan systems have a strong and sustained
581 sensitivity to orbital climate forcing over 10^4 to 10^5 year timescales, leaving behind a signal
582 that can be readily detected in basin sediments. The response timescale is an order of
583 magnitude shorter than the periodicity of glacial-interglacial cycles—at least in this debris flow-
584 dominated landscape with rapid source-to-sink sediment transfer—and there is no evidence
585 for significant signal shredding or buffering prior to deposition. The similarity of our results in
586 all 8 catchment-fan systems is evidence for reproducibility in an area where tectonic and

lithological boundary conditions are constant, and means all 35 dated fan surfaces can be combined to reconstruct a detailed time series of deposition during the past ~125 kyr.

Where does this climatic signal come from? Potential explanations include changes in sediment supply and/or mobilisation, and we explore both of these possibilities in sections 6.2 and 6.3. However, we first note that the changes in grain size are unlikely to be explained by post-depositional winnowing and alteration of the fan surfaces. In-situ processes could conceivably change the grain size distributions of these sediments after deposition. Weathering of large clasts could produce finer material and reduce the average grain size (although we avoided measuring obviously exfoliated sheets of granite, see Methods). Selective removal of fines or desert pavement formation could do the opposite, although we sampled gravels coarser than 1 mm so aeolian processes can be excluded, and desert pavement formation is minor. Ultimately, if the grain size changes in Fig. 8 were due to post-depositional effects, a very unlikely combination of variable rates and directions of grain size evolution would be required to explain how D_{50} could rapidly halve within 20 ka, remain relatively constant for a further 50 ka, before increasing again thereafter. Given the strong correlations between grain size and $\delta^{18}O$, which has itself fluctuated with an irregular pattern and a variable rate through time, the simplest interpretation is grain size is recording climate changes, and we proceed under this assumption.

6.2. Sediment source effects on grain size export to the fans

6.2.1. Transient exposure of moraines and glacial effects

Figures 10 and 11 characterise different sediment sources in two of the study catchments. Moraines and landslides export grain sizes that are only slightly coarser than the debris flows deposits, and one potential explanation for the grain size signal is that the relative contributions of these sources have changed over time. As shown by Fig. 11, the D_{50} of moraines is ~10 mm coarser than for landslides. However, given the amplitude of the changes in D_{50} over time (15 mm), moraine sediments would need to supply the majority of Q1 and Q4 sediments by volume for this to be a viable explanation.

We can use the Independence Creek and Symmes Creek catchments to place first-order constraints on the volumetric contributions of moraine sediments to the fans. These two catchments have moraines with total plan-view areas of 1.5 Mm^2 and 0.8 Mm^2, respectively (Fig. 1). If we assume that the entire moraine surfaces have been lowered at a time-averaged rate of 1 mm yr^{-1} since deglaciation at 18 ka, we estimate the respective volumes of moraine material exported to the fans to be ~27 Mm^3 and ~14 Mm^3. As a comparison we can estimate

621 the total volumes of mapped Q4 (post-glacial) sediments on the Independence Creek and
622 Symmes Creek fans by assuming an average thickness of 10 m (matching our field
623 observations, e.g., Fig. 3d) and multiplying this by their plan-view areas (Fig. 1), giving 114
624 Mm^3 and 208 Mm^3, respectively. In this scenario, the moraines would only have supplied
625 between 7 and 24% of the total Q4 volume. These are simple order-of-magnitude
626 approximations only, but even if a full quarter of the Q4 material was derived from moraines
627 (i.e., if the surfaces were lowering even faster than 1 mm yr^{-1}), the ~10 mm difference in D_{50}
628 (Fig. 11b) would still be diluted to a coarsening effect of only ~2 mm in the fan deposits,
629 demonstrating that moraine evacuation cannot explain the grain size changes we observed
630 on the fans.

631 Furthermore, we expect that releasing moraine material at the timing of deglaciation ~18 ka
632 ago (Rood et al., 2011) would generate an initial supply of coarse sediment that subsequently
633 would decay as the moraines are eroded and exported to the fans. Instead, we observe a
634 continued coarsening as the climate warmed, even long after deglaciation while moraines and
635 other paraglacial sediment sources are presumably being volumetrically depleted.
636 Additionally, the inset grain size-$\delta^{18}O$ plots in Fig. 8 show that the trajectory of grain size
637 change is the same regardless of whether the climate is cooling or warming. This is important,
638 because a lack of hysteresis (directionality in the signal) implies that the grain size supplied to
639 the fans is the same for a given temperature, irrespectively of whether glaciers are advancing
640 or retreating. In other words, all the potential sediment supply processes associated with
641 deglaciation (evacuation of moraines, enhanced landsliding, paraglacial supply, etc) appear
642 to have no detectable effect on the sensitivity and response of grain size to climate.

643 These considerations suggest that it is not possible for transient moraine erosion or paraglacial
644 sediment supply to explain the grain size changes shown in Fig. 8. Additionally, our study
645 catchments each experienced different spatial extents of glaciation in the past. Some of them
646 were fully glaciated right down to the fan apices (Birch Creek, Independence Creek), while
647 others were only glaciated in their upper reaches (e.g., Pinyon Creek, South Bairs Creek), and
648 consequently the moraine volumes in the catchments also vary (Fig. 1). Yet despite this, all 8
649 systems show similar grain size export through the glacial-interglacial cycle (Fig. 8) and cannot
650 be distinguished within uncertainty. This also implies that the intensity of glaciation in the
651 catchments does not exert a control on the grain size distributions of the fan deposits. Over-
652 steepened hillslopes in formerly glaciated parts of these catchments are undoubtedly
653 generating scree cones and debris (e.g., Fig. 3a, b; Fig. 10a), although the size distribution of
654 this material is mostly predetermined by bedrock jointing and there is no evidence this has
655 changed in phase with climate throughout the last 125 kyr.

Figure 11a also shows measured grain size distributions for scree cones in the Independence Creek and Symmes Creek catchments. Scree cones provide large, metre-scale blocks and little finer material (see also Fig. 10b), and their grain size distributions only marginally overlap with those measured on the fans. The changes in D_{50} and D_{84} we document in Fig. 8 reflect systematic shifts in the grain size distributions across all particle sizes on the fans, and cannot be explained by only increasing or decreasing the supply of very coarse material (see Fig. 4). Given that scree cones deliver so little gravel (Figs 10b and 11a), we expect that significantly changing their volumetric contributions to the fans would act to change the shapes of the grain size distributions in Fig. 4, and extend their long tails in a way we do not observe in any of the deposits. There is also no evidence that very large blocks can be crushed into gravel over such short transport distances (Fig. 6). Furthermore, the same arguments apply about the lack of hysteresis in the grain size-$\delta^{18}O$ records and the sustained coarsening long after deglaciation (Fig. 8). For example, if deglaciation exposed more scree cones in the catchments, this effect would need to continue increasing throughout the Holocene long after the glaciers retreated, and is also undetectable when grain size is plotted against the $\delta^{18}O$ record (Fig. 8, inset panels).

In summary, the sustained coarsening long after deglaciation; the lack of hysteresis and directionality in the grain size-$\delta^{18}O$ plots; and the consistency of the grain size changes in all 8 fans despite differences in past glaciation, together lead us to conclude that paraglacial sediment supply cannot be the primary explanation for the data in Fig. 8. The shapes of the grain size distributions measured on the fans, as well as the specific timings of grain size changes we observe in Fig. 8, indicate that changing the supply of sediment from coarse-grained scree cones cannot explain our observations from the fan deposits either. More fundamentally, whatever the grain sizes supplied from the hillslopes, all this material still has to be transported to the fans for any effect to be captured in the debris flow deposits.

6.2.2. Changes in grain size production by weathering

Additionally, the grain size distribution of sediment simply generated on hillslopes by weathering could have changed as a direct result of climate fluctuations during the last 125 kyr. For example, sediment with a longer hillslope residence time tends to be finer-grained as a result of prolonged chemical and physical weathering (Attal et al., 2015), and the fragmentation of particles plays an important role in setting grain size distributions (Allen et al., 2015). Today, our target catchments experience strong orographic gradients in climate, as a result of ~2000 m topographic relief and the rain shadow imposed by the Sierra Nevada. From the tops of the catchments to the fans, temperature varies by >15 °C and precipitation

691 rate decreases by a factor of ~4 from almost 1000 mm yr^{-1} to <250 mm yr^{-1} (Fig. 4b). This
692 spatial gradient in climate is more than twice as extreme as the amplitude of glacial-interglacial
693 climate fluctuations, which are 5-6 °C and a factor of ~2 for average precipitation rate (see
694 Study Area). Therefore, if such gradients in climate are capable of generating grain size
695 differences of 10s of mm in weathered material (sufficient to explain the fan deposits), then
696 this effect must be apparent in the catchments orographically today.

697 Fortunately, prior work has characterised the production of different grain size fractions of
698 sediment, by weathering and as a function of elevation, in the Inyo Creek catchment (Stock et
699 al., 2006; Riebe et al., 2015). Inyo Creek lies just 10 km south of George Creek on the eastern
700 front of the range, drains the same topographic relief, experiences identical climatic and
701 tectonic conditions, and erodes the same granitic bedrock units, making it an ideal
702 comparison. It was never glaciated, meaning sediment production by weathering can be
703 investigated in isolation (Stock et al., 2006). These studies used detrital thermochronometry
704 as a tracer to identify the source elevations of different gravel grain size fractions exported
705 into Owens Valley. Their results show that coarser gravel (D_{50} ~40 mm) is preferentially
706 produced at higher elevations (between ~2.75 km and 4 km elevation) in the periglacial zone
707 dominated by physical weathering processes and with barren hillslopes, frequent landsliding,
708 little soil development, and where particles have a short residence time (Riebe et al., 2015).
709 Conversely, finer gravel (D_{50} ~10 mm) is preferentially produced at lower elevations (between
710 2 and 3 km), below the tree line in the vegetated part of the eastern Sierra Nevada where
711 there is soil production, and where particles have a longer residence time and prolonged
712 exposure to chemical weathering (Stock et al., 2006; Riebe et al., 2015). These findings agree
713 with other constraints from the Sierra Nevada (Dixon et al., 2009; Attal et al., 2015; Sklar et
714 al., 2016) and together show that sediment supply—and grain size production in particular—
715 varies as a function of elevation, with coarser material generated at higher elevations in the
716 catchments.

717 The production of different grain sizes by weathering may have occurred at different elevations
718 under glacial conditions, because the weathering and orographic climate conditions were
719 different compared to today. Local pollen data from Owens Valley show that the periglacial
720 conditions now found at the top of the range expanded downslope, displacing the tree-line to
721 elevations 500-600 m lower than at present (Woolfenden, 2003). A larger pollen database
722 compiled for the SW United States shows very similar results (Pelletier, 2014), implying this
723 was a regional response to the glacial climate. Consequently, the periglacial zone where
724 coarser particles are known to be generated in this landscape (Stock et al., 2006; Riebe et al.,
725 2015; Sklar et al., 2016) was expanded, implying that slightly more coarse-grained sediment

was being generated during the glacial period. This cannot be reconciled with the ~15 mm of fining in D_{50} that we observe on the fans at the LGM (Fig. 8).

As such, we propose that it is not possible to explain the grain size variations on the fans (Fig. 8) by invoking changes in weathering and grain size production in the catchments. At the LGM we expect a slight increase in coarse gravel production due to depression of the vegetated zone and expansion of the periglacial zone where coarser material is supplied. The amplitude of the orographic climate gradient in these catchments is much larger than the amplitude of glacial-interglacial climate variability, so it is reasonable to look at spatial climate gradients to test this. However, while changes in the grain size sources cannot explain the data in Fig. 8, this does mean that the availability of a wide range of grain sizes for export to the fans is not a limiting factor in these catchments. Indeed, whatever the grain size supplied by any source of sediment in these catchments, all of this material still needs to be mobilised and transported to the fans, and this process may be size-selective.

6.3. Explanations involving sediment transport

Another potential explanation for glacial-interglacial grain size variability is that the ability of debris flows to mobilise and deposit coarser particles has increased as the climate warmed. Documented debris flows in this study area are runoff-induced events triggered by intense storm rainfall (DeGraff et al., 2011). There are still uncertainties about how to describe the initiation of debris flows by surface runoff (and other mechanisms) mathematically (Kean et al., 2013; Rengers et al., 2016), and associated transport laws that specifically deal with grain size incorporation do not yet exist. Nonetheless, the initiation of debris flows by runoff has been observed widely in the field (Coe et al., 1997; Cannon et al., 2001, 2008; DeGraff et al., 2011; Kean et al., 2011; Hobley et al., 2012; Staley et al., 2014), including video footage (Kean et al., 2013); it has been studied with laboratory experiments (Gregoretti, 2000); and it can be realistically simulated with process-based modelling (Kean et al., 2013; Rengers et al., 2016). These studies confirm that debris flows can be triggered when sediment is mobilised from hillslopes by intense surface runoff (without a discrete spatial point of initiation), at least in alpine landscapes where the supply of loose sediment is abundant (Kean et al., 2013; Staley et al., 2014; Rengers et al., 2016). Consequently, empirical thresholds of rainfall intensity/duration required for debris flow initiation can be described for a given landscape (e.g., Cannon et al., 2008; Guzzetti et al., 2008). Also, as they are threshold-limited events their deposits may not record information about average climate conditions, but instead document changes in extreme rainfall.

We hypothesise that the grain size trends in Fig. 8 record an increase in threshold-surpassing storm intensities with warming, and an associated increase in the surface runoff provided for the initiation of debris flows, which has therefore led to deposits that are coarser-grained on average. As the glacial period was wetter than the Holocene, this explanation would imply that changes in the uppermost percentiles of rainfall intensity are decoupled from changes in mean annual precipitation, as is frequently the case (cf., Trenberth, 2011). In other words, the regional climate has become drier overall with warming, but we expect the highest-magnitude storms responsible for initiating debris flows to have intensified at the same time.

6.3.1. Changes in storm rainfall intensity

Glacial-interglacial time series of past storm intensity do not exist, but there is much we do know from modern climate dynamics. It is well-documented that as temperature increases the intensity of storm rainfall (defined as the uppermost percentiles of rainfall rate, e.g., P_{99}) generally increases, because the capacity of the atmosphere to hold moisture rises exponentially with temperature (Trenberth et al., 2003; Wentz et al., 2007; Allan & Soden, 2008; Lenderink & Meijgaard, 2008, 2010; Berg et al., 2009, 2013; Liu et al., 2009). This is described by the Clausius-Clapeyron (CC) relationship, where the moisture-holding capacity of the atmosphere increases by approximately 7% per 1°C of warming, resulting in an equivalent increase in the upper percentiles of storm rainfall intensity with temperature (Trenberth et al., 2003; Berg et al., 2009; Trenberth, 2011). This has been consistently documented for (i) a variety of climatic settings; (ii) a wide range of temperatures (~0-30°C); (iii) the uppermost percentiles of extreme rainfall likely to trigger debris flows; and (iv) a variety of storm types, i.e., thunderstorms, tropical cyclones, and extratropical rainstorms (Hardwick Jones et al., 2010; Lenderink et al., 2011; Shaw et al., 2011; Utsumi et al., 2011; Berg et al., 2013). It therefore reflects the fundamental physics of storm rainfall (Trenberth, 2011). Trenberth et al. (2003) observed that in some vigorous storms the rate of increase in rainfall intensity with temperature can slightly exceed Clausius-Clapeyron. For short-lived and deeply convective storms occurring in warm conditions, such as the local thunderstorms that strike Owens Valley during the summer and autumn, the rate can be up to twice Clausius-Clapeyron, i.e., 14% per 1°C of warming (Liu et al., 2009; Berg et al., 2013; Singleton and Toumi, 2013). Additionally, more intense precipitation events occur in a warmer climate, even if mean annual precipitation rate declines (cf., Trenberth, 2011).

Climate changes during the last glacial-interglacial cycle are captured in detail by the sea surface temperature record of Yamamoto et al. (2007) from offshore California (Fig. 5). This ODP-1016 record offers an opportunity to compare our grain size measurements with

795 temperature as a primary climatic variable, in addition to proxies like $\delta^{18}O$ explored earlier.
796 This is especially true given that sea surface temperature is strongly related to the total amount
797 of precipitable water in the atmosphere over the oceans (Trenberth et al., 2005), and that
798 moisture delivered to the study area originates in the Pacific (Fig. 4a).

799 We plot grain size directly against this sea surface temperature record in Fig. 12, with D_{50}
800 (black) and D_{84} (red) displayed for debris flow channels and levees separately. As expected,
801 grain size varies systematically with temperature as the climate cooled and warmed by a total
802 amplitude of ~6°C during the last 125 kyr. The coarsest material was deposited when the
803 climate was warm during the current and last interglacials, and the finest material was
804 deposited when temperatures were lowest during the LGM. The best fits to the data are with
805 exponential regressions, which are shown for the stratigraphic averages (stars) and appear
806 linear because the *y*-axis is logged. The rate of grain size coarsening with warming lies
807 between 9.0 and 13.7% per 1°C of warming. If the true value of this rate is assumed to be the
808 same for all four data series, then the standard errors tolerate a range of 9.9-10.4% per 1°C
809 (i.e., all four data sets overlap, within uncertainty, at a rate of ~10% per 1°C). Significantly,
810 these constraints lie directly between the CC and 2 x CC rates of 7 and 14% per 1°C
811 respectively, that generally describe the intensification of storm rainfall rates with warming
812 (Trenberth et al., 2003; Berg et al., 2009, 2013; Hardwick Jones et al., 2010; Lenderink et al.,
813 2011; Trenberth, 2011; Utsumi et al., 2011).

814 There is a strong correlation between the rate of debris flow grain size coarsening in Owens
815 Valley, and the rate at which storm rainfall intensity generally increases with temperature, over
816 a range of >5°C. This does not prove cause and effect; indeed cause and effect cannot be
817 proven without an independent proxy of storm intensity, which does not exist. However, we
818 propose that this sustained exponential pattern of grain size coarsening, which mimics the
819 Clausius-Clapeyron relationship, is unlikely to be coincidental. This is especially the case
820 given that: (i) these debris flows are known to be threshold-limited events directly triggered by
821 storm runoff; (ii) there is a clear lack of hysteresis; and (iii) the grain size response to climate
822 forcing is instantaneous at the temporal resolution of our data. Even within modern records of
823 climate variability, the intensities of storms affecting our study area correlate with warmer
824 Pacific surface temperatures (Persson et al., 2005; Antinao & McDonald, 2013a). The most
825 extreme flooding in Owens Valley is caused by summer and autumn thunderstorms delivering
826 moisture from the tropical Pacific (Kattelmann, 1992), and for these kinds of localised
827 convective storms the rainfall intensity-temperature scaling may slightly exceed Clausius-
828 Clapeyron, often estimated at 10-14% per 1°C (Lenderink & Meijgaard, 2008; Liu et al., 2009;
829 Berg et al., 2013; Singleton & Toumi, 2013).

6.3.2. Particle mobility

Our findings suggest a direct, causative link between storm rainfall intensity and the grain sizes deposited on these debris flow fans (see section 6.3.1); here we explore how such a link may come about.

How can it be that particle diameters of several 10s of mm can be limited by surface runoff, when these debris flows are obviously able to move much larger boulders (e.g., Fig. 3)? We actually observe a coarsening throughout the entire grain size distribution in response to warming (Fig. 7), which applies to the coarsest material as well as the finest, and not exclusively to the 10-100 mm size fraction (i.e., D_{50} is simply a percentile). Debris flows are known to move in characteristic surges, which are capable of carrying large particles due to the mechanical properties of granular mass flows, including kinetic sieving and the nature of the vertical velocity profile (Bagnold, 1954; Iverson, 1997; Gray and Thornton, 2005; Gray and Kokelaar, 2010; Johnson et al., 2012). However these surges are not necessarily responsible for setting the grain size distribution of the deposits. Our observations in Fig. 6 indicate that once a viscous debris flow has formed in this environment, grain size changes by relatively little over a 10 km distance, at least where observed on the fans (Fig. 6). This leaves the question of when and where much of the sediment is incorporated into a debris flow and how the grain size distribution of that material is established.

One study that addresses the initiation of debris flows by storm runoff is by Kean et al. (2013), who document a variety of flow events in California and Colorado. They observed that intense runoff creates many small granular flows that converge throughout a catchment. A large amount of the bedload sediment assimilated into a debris flow is initially mobilised by surface runoff on hillslopes, with coarser particles assumed to be mobilised by greater surface runoff rates. Surface runoff moves this sediment down-slope and into sediment traps, in which large debris flows nucleate and directly inherit this material. This initiation mechanism may apply in our study catchments, as (i) debris flows are known to be triggered by storm runoff (DeGraff et al., 2011); (ii) there is abundant loose sediment available on the hillslopes with a wide range of grain sizes available (Figs 10 and 11); and (iii) past glaciation has created stepped long profiles that may act as sediment traps (Figs 2 and 9), in addition to sediment traps in the main channels (Fig. 10e-f). Therefore, one potential explanation for the grain size data is that the peak rainfall intensity of storms increased with warming, leading to an increase in instantaneous surface runoff rates on hillslopes, mobilising an overall coarser grain size distribution of sediment that is then inherited by large and viscous debris flows. This would explain the Clausius-Clapeyron-style relationship between grain size and past temperature

(Fig. 12), while also conforming to observations about how runoff-generated debris flows are initiated (Kean et al., 2013; Rengers et al., 2016). Kean et al. (2013) combine their observations from California and Colorado with physical theory in order to develop a model of flow initiation, and find that storm water discharge is an essential parameter for accurately simulating real debris flow surges. Furthermore, these authors compare debris flows initiated by storms with different peak rainfall intensities. They find that the power and volume of debris flow surges increases in response to greater peak storm rainfall intensity. Therefore, even if additional material is entrained by debris flow surges after initiation by surface runoff, more powerful surges might still entrain larger particles. Alternatively, some debris flows in this landscape may be initiated by the failure of saturated sediment on hillslopes during intense storms (e.g., Hubert and Filipov, 1989; Iverson, 1997), and this will still be promoted by increased rainfall intensities.

Our observations from the Owens Valley fans indicate that: (i) these debris flows exhibit particle size selectivity that varies in concert with past climate change; (ii) there is little down-system change in grain size after a debris flow has formed, implying that sediment deposition is not predominantly size-selective; and (iii) any entrainment of material into the debris flows during transport on the fans is not significantly altering the grain size distributions.

6.3.3. Debris flow initiation and storm intensities

If our hypothesis is correct, and the storms that trigger debris flows in the Owens Valley region have intensified with warming, then we should be able to evaluate this using known debris flow initiation thresholds for rainfall intensity and duration. If storm intensity is down-scaled following the Clausius-Clapeyron relationship for a realistic LGM temperature anomaly, storms must still surpass these thresholds for debris flow initiation (because we know that debris flows occurred). However if this results in an unreasonably large drop in storm intensity—falling below the threshold for initiating debris flows—then this mechanism cannot work given the known debris flow activity recorded by the fans.

We perform this simple test in Fig. 13, which shows rainfall intensity against duration over four orders of magnitude, making the assumption that debris flow initiation thresholds do not significantly change over time. The main storm systems affecting Owens Valley are highlighted in blue after Antinao and McDonald (2013a), and various initiation thresholds are plotted as black lines based on detailed observational datasets (after Cannon et al., 2008 and Guzzetti et al., 2008). As expected, shorter-lived storms need to be more intense in order to trigger a debris flow, with a 1 hour event (e.g., a summer thunderstorm) triggering a debris flow if rainfall intensity reaches ~10 mm hr^{-1}, but for a storm lasting a day or longer lower intensities are

sufficient. With red circles, we have plotted three examples of storms in recent years that were observed to trigger debris flows in our study area and neighbouring catchments, and for which there are precise constraints on rainfall intensity and duration. All three events were initiated by summer thunderstorms, as is typical for historical debris flows in Owens Valley (Hubert and Filipov, 1989; Blair and McPherson, 1998). The Erskine Creek and Oak Creek debris flows both occurred on 12th July 2008 and are described by DeGraff et al. (2011); they were triggered by peak rainfall intensities of 16-20 mm hr^{-1} sustained for ~15 minutes (Erskine Creek) and 25-32 mm hr^{-1} sustained for ~40 minutes (Oak Creek). Another debris flow occurred in North Bairs Creek on 22nd July 2013. We characterised the triggering storm using NEXRAD Doppler weather radar data (freely available courtesy of NOAA at: https://www.ncdc.noaa.gov/data-access/radar-data/nexrad) as having a peak rainfall intensity of 20-30 mm hr^{-1} sustained for 10-30 minutes. As expected, these storms lie above debris flow initiation thresholds that are likely to be suitable for the Owens Valley area (Fig. 13).

If we assume these storms are representative of modern debris flow-triggering events, we can down-scale their intensities following the CC and 2x CC rates (7 and 14% per 1°C) by a drop in temperature of 5°C, which is representative of the LGM. This is shown on Fig. 13 with green and blue symbols, respectively. This illustrates the magnitude of glacial-interglacial variations in peak storm intensity that we are hypothetically invoking, as a function of temperature, via the Clausius-Clapeyron scaling. We scale up the durations of the storms by the same CC and 2x CC rates. This is because the propagation velocity of a storm front may also increase with temperature at a CC to 2x CC rate (Singleton and Toumi, 2013). In other words, in a colder LGM scenario a typical storm could migrate over a given stationary point on the surface more slowly than in a warmer modern scenario, increasing the duration of the storm experienced at that location. The results show that, adjusting rainfall intensity-duration to a 5 ºC temperature decrease, according to either Clausius-Clapeyron or twice this rate, would still generate intensities that fall above known debris flow initiation thresholds. This means that invoking changes in storm rainfall intensity, in order to explain the observed grain size changes through time, does not require such a large decrease in intensity that debris flows could not be initiated, but still satisfies Fig. 12. This offers a simple first-order sense check of our interpretations, and implies the required changes in storm intensity occupy a narrow window of suitable variation. Our hypothesis therefore reconciles with (i) known climate dynamics; (ii) known debris flow initiation thresholds; (iii) grain size observations from the fans; and (iv) known debris flow activity throughout the glacial period as well as today.

6.4. Implications and future challenges

Our findings confirm that alluvial fan deposits, in this setting, record glacial-interglacial climate changes over 10^4 to 10^5 year timescales. One striking observation is that as the climate warmed and dried overall, the grain size exported to fans became coarser, in contrast to numerical models of catchment-fan systems that typically predict a fining due to decreased discharge (e.g., Paola et al., 1992; Armitage et al., 2011; Simpson and Castelltort, 2012; Allen et al., 2013). Fundamentally, our data demonstrate the palaeoclimatic significance of alluvial fan stratigraphy and we propose that debris flow deposits may preserve a record of past changes in storm rainfall intensity. The response timescale of these systems is rapid and effectively instantaneous at the temporal resolution of our data. This indicates that efficient depositional processes like debris flows pre-condition sediment routing systems for climatic sensitivity, by quickly transferring sediment to the basin. As our analyses show, the grain size signal can be plausibly explained by the importance of high-intensity storm events, which are likely to have increased with warming in our study area, decoupled from the overall rainfall budget. Therefore, this study also underscores the need to understand the intensity distribution of precipitation and how this affects landscape processes, because climate change can have opposing effects on the upper percentiles of rainfall intensity compared to averages.

Of course, grain size is not the only way these deposits can (or should) be quantified, and further work could measure other parameters such as depositional volumes or (palaeo)erosion rates. For grain size in particular, there is an opportunity to develop new mechanical models for describing runoff-induced debris flows that specifically link the grain size distributions mobilised and deposited with surface runoff rates and the physics of debris flow transport. These transport laws are currently unknown, but would enable real progress in understanding the sedimentary record of debris flows and landscape evolution in general.

Furthermore, we find that the grain size response to climate change may be non-linear and accelerates with warming, as implied by the regressions in Figs 8 and 12. If this is the case, and this trend continues with future warming, then an even greater sensitivity of debris flows to climate might be expected. Existing ideas about debris flow erosion (e.g., Stock and Dietrich, 2006) suggest that flows with larger particles will themselves be more erosive, potentially leading to an erosional feedback in the landscape.

7. Conclusions

By measuring sedimentary grain size distributions in detail (>30,000 clasts on 35 dated surfaces), we show that debris flow fans in Owens Valley, California are highly sensitive to glacial-interglacial climate variability over the last ~125 kyr, recording known climate shifts in alluvial fan stratigraphy. As the climate warmed by 5-6°C from the LGM to the present day, total rainfall halved but storm rainfall intensity likely increased, and measured D_{50} and D_{84} grain size percentiles approximately doubled. The correlation between grain size and climate is sustained throughout the entire last glacial-interglacial cycle, with a clear exponential scaling between grain size and sea surface temperatures from offshore California. The form of this scaling, with a grain size coarsening rate of ~10% per 1°C, mimics the Clausius-Clapeyron relationship and closely matches how storm rainfall intensity scales with temperature (Lenderink & Meijgaard, 2008; Liu et al., 2009; Trenberth, 2011; Berg et al., 2013). We therefore propose that debris flow stratigraphy in these systems records changes in storm rainfall intensity during the last glacial-interglacial cycle. Our findings are reproducible in 8 different catchment-fan systems with precise age control and where tectonic and lithological boundary conditions are uniform.

These systems have a rapid response timescale that is shorter than the minimum temporal resolution of our data, and show no evidence of signal damping, demonstrating that this debris flow-dominated landscape has a high sensitivity to past climate changes over 10^4 to 10^5 year timescales. By characterising sediment sources in the parent catchments, we demonstrate that neither the transient erosion of moraine sediments nor other paraglacial sediment supply processes are likely to explain the grain size changes observed on the fans. Similarly, we use constraints on sediment production as a function of elevation to show that altitudinal changes in hillslope weathering are unlikely to explain the grain size changes either. The sustained correlation between grain size and climate, the lack of hysteresis in the response to climate change, and the timings of the grain size response, together lead us to conclude that changes in sediment sources do not drive the grain size sensitivity to climate in this setting.

Instead, we conclude that as the climate warmed and dried overall the intensity of high-magnitude storms is likely to have increased, leading to greater surface runoff rates that entrained coarser sediment during debris flow initiation. This interpretation is supported by (i) expectations from climate dynamics; (ii) the mechanics of debris flow initiation by runoff; (iii) a Clausius-Clapeyron-style exponential scaling between grain size and past temperature that matches the expected pattern for storm rainfall intensity; (iv) modern observations about the storms that do trigger these debris flows, as well as the rainfall intensity-duration thresholds required. Our findings provide useful constraints for future attempts to develop a debris flow

transport model that explicitly accounts for grain size incorporation into flows and deposits. Additionally, this study underscores the importance of distinguishing between rainfall intensity and total amount in geomorphic analyses. Finally, we highlight the potential risk of continued climate warming in the near future, which we predict could trigger coarser-grained, more erosive and more hazardous debris flows in this landscape.

8. Acknowledgements

MD and DRB received generous financial support from the Janet Watson bursary scheme at the Department of Earth Science and Engineering, Imperial College London. MD also thanks the British Society for Geomorphology, the Geological Society of London, the International Association of Sedimentologists and the Jeremy Willson Charitable Trust for grants that financed field work. ACW was supported by the Royal Society. The authors thank Alexander Densmore and Daniel Hobley for detailed reviews that improved the manuscript.

9. References

Allan, R.P. & Soden, B.J. (2008) Atmospheric warming and the amplification of precipitation extremes. *Science*, **321**, 1481-1484.

Allen, P.A. & Densmore, A.L. (2000) Sediment flux from an uplifting fault block. *Basin Research*, **12**, 367-380.

Allen, P.A. (2008) From landscapes into geological history. *Nature*, **451**, 274-276.

Allen, P.A., Armitage, J.J., Carter, A., Duller, R.A., Michael, N.A., Sinclair, H.D., Whitchurch, A.L. & Whittaker, A.C. (2013) The Qs problem: Sediment volumetric balance of proximal foreland basin systems. *Sedimentology*, **60**, 102-130.

Allen, P.A., Armitage, J.J., Whittaker, A.C., Michael, N.A., Roda-Boluda, D.C. & D'Arcy, M. (2015) Fragmentation model of the grain size mix of sediment supplied to basins. *The Journal of Geology,* **123**, 405-427.

Antinao, J.L. & McDonald, E. (2013a) An enhanced role for the tropical Pacific on the humid Pleistocene-Holocene transition in southwestern North America. *Quaternary Science Reviews*, **78**, 319-341.

Antinao, J.L. & McDonald, E. (2013b) A reduced relevance of vegetation change for alluvial aggradation in arid zones. *Geology*, **41**, 11-14.

1031 Armitage, J.J., Duller, R.A., Whittaker, A.C. & Allen, P.A. (2011) Transformation of tectonic
1032 and climatic signals from source to sedimentary archive. *Nature Geoscience,* **4**, 231-235.

1033 Armitage, J.J., Dunkley Jones, T., Duller, R.A., Whittaker, A.C. & Allen, P.A. (2013) Temporal
1034 buffering of climate-driven sediment flux cycles by transient catchment response. *Earth and*
1035 *Planetary Science Letters,* **369-370**, 200-210.

1036 Attal, M., Mudd, S.M., Hurst, M.D., Weinman, B., Yoo K. & Naylor, M. (2015) Impact of change
1037 in erosion rate and landscape steepness on hillslope and fluvial sediments grain size in the
1038 Feather River basin (Sierra Nevada, California). *Earth Surface Dynamics,* **3**, 201-222.

1039 Bagnold, R.A. (1954) Experiments on a gravity-free dispersion of large solid spheres in a
1040 Newtonian fluid under shear. *Proceedings of the Royal Society A*, **225**, 49-63.

1041 Beaty, C.B. (1963) Origin of alluvial fans, White Mountains, California and Nevada. *Annals of*
1042 *the Association of American Geographers*, **53**, 516-535.

1043 Bekaddour, T., Schlunegger, F., Vogel, H., Delunel, R., Norton, K.P., Akçar, N. & Kubik P.
1044 (2014) Paleo erosion rates and climate shifts recorded by Quaternary cut-and-fill sequences
1045 in the Pisco valley, central Peru. *Earth and Planetary Science Letters,* **390**, 103-115.

1046 Benson L.V., Burdett J.W., Kashgarian M., Lund S.P., Phillips F.M., & Rye R.O. (1996)
1047 Climatic and hydrologic oscillations in the Owens Lake basin and adjacent Sierra Nevada,
1048 California. *Science,* **274**, 746-749.

1049 Berg, P., Haerter, J.O., Thejll, P., Piani, C., Hagemann, S. & Christensen, J.H. (2009)
1050 Seasonal characteristics of the relationship between daily precipitation intensity and surface
1051 temperature. *Journal of Geophysical Research*, **114**, D18102.

1052 Berg, P., Moseley, C. & Haerter, J.O. (2013) Strong increase in convective precipitation in
1053 response to higher temperatures. *Nature Geoscience*, **6**, 181-185.

1054 Bierman, P., Gillespie, A., Whipple, K. & Clark, D. (1991) Quaternary geomorphology and
1055 geochronology of Owens Valley, California: Geological Society of America Field Trip. In:
1056 *Geological excursions in southern California and Mexico: guidebook for the 1991 annual*
1057 *meeting. Geological Society of America, San Diego* (pp. 199-223).

1058 Bischoff, J.L., Menking, K.M., Fitts, J.P. & Fitzpatrick, J.A. (1997) Climatic oscillations 10,000-
1059 155,000 yr B.P. at Owens Lake, California reflected in glacial rock flour abundance and lake
1060 salinity in Core OL-92. *Quaternary Research*, **48**, 313-325.

1061 Blackwelder, E. (1928) Mudflow as a geologic agent in semiarid mountains. *Geological Society*
1062 *of America Bulletin*, **39**, 465-484.

1063 Blair, T.C. and McPherson, J.G. (1998) Recent debris-flow processes and resultant form and
1064 facies of the Dolomite alluvial fan, Owens Valley, California. *Journal of Sedimentary Research*,
1065 **68**, 800-818.

1066 Blum, M.D. & Törnqvist, T.E. (2000) Fluvial responses to climate and sea-level change: a
1067 review and look forward. *Sedimentology,* **47**, 2-48.

1068 Bonnet, S. & Crave, A. (2003) Landscape responses to climate change: Insights from
1069 experimental modeling and implications for tectonic versus climatic uplift of topography.
1070 *Geology,* **31**, 123-126.

1071 Bookhagen, B. & Strecker, M.R. (2012) Spatiotemporal trends in erosion rates across a
1072 pronounced rainfall gradient: Examples from the southern Central Andes. *Earth and Planetary*
1073 *Science Letters*, **327-328**, 97-110.

1074 Brocklehurst, S.H., Whipple, K.X. & Foster, D. (2008) Ice thickness and topographic relief in
1075 glaciated landscapes of the western USA. *Geomorphology*, **97**, 35-51.

1076 Bull, W.B. (1991) *Geomorphic responses to climate change*. Oxford University Press, New
1077 York, USA, pp. 326.

1078 Burke, K., Francis, P. & Wells, G. (1990) Importance of the geological record in understanding
1079 global change. *Palaeogeography, Palaeoclimatology, Palaeoecology*, **89**, 193-204.

1080 Cannon, S.H., Gartner, J.E., Wilson, R.C., Bowers, J.C. & Laber, J.L. (2008) Storm rainfall
1081 conditions for floods and debris flows from recently burned areas in southwestern Colorado
1082 and southern California. *Geomorphology*, **96**, 250-269.

1083 Cannon, S.H., Kirkham, R.M. and Parise, M. (2001) Wildfire-related debris-flow initiation
1084 processes, Storm King Mountain, Colorado. *Geomorphology*, **39**, 171-188.

1085 Castelltort, S. & Van Den Driessche, J. (2003) How plausible are high-frequency sediment
1086 supply-driven cycles in the stratigraphic record? *Sedimentary Geology,* **157**, 3-13.

1087 Champagnac, J-D., Molnar, P., Sue, C. & Herman, F. (2012) Tectonics, climate, and mountain
1088 topography. *Journal of Geophysical Research,* **117**, B02403.

1089 Clark, M.K., Maheo, G., Saleeby, J. & Farley, K.A. (2005) The non-equilibrium landscape of
1090 the southern Sierra Nevada, California. *Geological Society of America Today*, **15**, 4-10.

1091 Clarke, L., Quine, T.A. & Nicholas, A. (2010) An experimental investigation of autogenic
1092 behaviour during alluvial fan evolution. *Geomorphology,* **115**, 278-285.

1093 Coe, J.A., Glancy, P.A. and Whitney, J.W. (1997) Volumetric analysis and hydrologic
1094 characterization of a modern debris flow near Yucca Mountain, Nevada. *Geomorphology*, **20**,
1095 11-28.

1096 Coe, J.A., Kinner, D.A. & Godt, J.W. (2008) Initiation conditions for debris flows generated by
1097 runoff at Chalk Cliffs, central Colorado. *Geomorphology*, **96**, 270-297.

1098 COHMAP members (1988) Climatic changes of the last 18,000 years: Observations and
1099 model simulations. *Science*, **241**, 1043-1052.

1100 D'Arcy, M. & Whittaker, A.C. (2014) Geomorphic constraints on landscape sensitivity to
1101 climate in tectonically active areas. *Geomorphology,* **204**, 366-381.

1102 D'Arcy, M., Roda Boluda, D.C., Whittaker, A.C. & Carpineti, A. (2015) Dating alluvial fan
1103 surfaces in Owens Valley, California, using weathering fractures in boulders. *Earth Surface*
1104 *Processes and Landforms,* **40**, 487-501.

1105 D'Arcy, M., Whittaker, A.C. & Roda-Boluda, D.C. (2016) Measuring alluvial fan sensitivity to
1106 past climate changes using a self-similarity approach to grain-size fining, Death Valley,
1107 California. *Sedimentology*, in press, doi: 10.1111/sed.12308.

1108 DeGraff, J., Wagner, D., Gallegos, A., DeRose, M., Shannon, C. & Ellsworth, T. (2011) The
1109 remarkable occurrence of large rainfall-induced debris flows at two different locations on July
1110 12, 2008, Southern Sierra Nevada, CA, USA. *Landslides*, **8**, 343-353.

1111 Densmore, A.L., Allen, P.A. and Simpson, G. (2007) Development and response of a coupled
1112 catchment fan system under changing tectonic and climatic forcing. *Journal of Geophysical*
1113 *Research,* **112**, F01002.

1114 Dixon J.L, Heimsath A.M, Amundson R. (2009) The critical role of climate and saprolite
1115 weathering in landscape evolution. *Earth Surface Processes and Landforms,* **34**, 1507-1521.

1116 Dühnforth M., Densmore A.L., Ivy-Ochs S., Allen P.A., Kubik P.W. (2007) Timing and patterns
1117 of debris flow deposition on Shepherd and Symmes creek fans, Owens Valley, California,
1118 deduced from cosmogenic ^{10}Be. *Journal of Geophysical Research: Earth Surface* **112**,
1119 F03S15.

1120 Dühnforth M., Densmore A.L., Ivy-Ochs, S. & Allen, P.A. (2008) Controls on sediment
1121 evacuation from glacially modified and unmodified catchments in the eastern Sierra Nevada,
1122 California. *Earth Surface Processes and Landforms*, **33**, 1602-1613.

Duller, R.A., Whittaker, A.C., Fedele, J.J., Whitchurch, A.L., Springett, J., Smithells, R., Fordyce, S. and Allen, P.A. (2010) From grain size to tectonics. *Journal of Geophysical Research,* **115**, F03022.

Fernandes, N.F. & Dietrich, W.E. (1997) Hillslope evolution by diffusive processes: The timescale for equilibrium adjustments. *Water Resources Research*, **33**, 1307-1318.

Foreman, B.Z. (2014) Climate-driven generation of a fluvial sheet sand body at the Paleocene-Eocene boundary in north-west Wyoming (USA). *Basin Research,* **26**, 225-241.

Foreman, B.Z., Heller, P.L. and Clementz, M.T. (2012) Fluvial response to abrupt global warming at the Palaeocene/Eocene boundary. *Nature,* **491**, 92-95.

Fuchs, M., Reverman, R., Owen, L.A. and Frankel, K.L. (2015) Reconstructing the timing of flash floods using ^{10}Be surface exposure dating at Leidy Creek alluvial fan and valley, White Mountains, California-Nevada, USA. *Quaternary Research*, **83**, 178-186.

Gesch, D.B., Oimoen, M., Greenlee, S.K., Nelson, C., Steuck, M. and Tyler, D. (2002) The National Elevation Dataset. *Photogrammetric Engineering and Remote Sensing,* **68**, 5-11.

Gillespie, A.R. (1982) *Quaternary glaciation and tectonism in the Southeastern Sierra Nevada*. Ph.D. thesis, California Institute of Technology, Pasadena, CA, USA, pp. 720.

Gray, J.M.N.T. and Thornton, A.R. (2005) A theory for particle size segregation in shallow granular free-surface flows. *Proceedings of the Royal Society A*, **461**, 1447-1473.

Gray, J.M.N.T. and Kokelaar, B.P. (2010) Large particle segregation, transport and accumulation in granular free-surface flows. *Journal of Fluid Mechanics*, **652**, 105-137.

Gregoretti, C. (2000) Experimental evidence from the triggering of debris flow along a granular slope. *Physics and Chemistry of the Earth, Part B: Hydrology, Oceans and Atmosphere*, **25**, 387-390.

Guzzetti, F., Preuccacci, S., Rossi, M. & Stark, C.P. (2008) The rainfall intensity-duration control of shallow landslides and debris flows: an update. *Landslides*, **5**, 3-17.

Hallet, B. (1990) Spatial self-organization in geomorphology: from periodic bedforms and patterned ground to scale-invariant topography. *Earth-Science Reviews,* **29**, 57-75.

Hardwick Jones, R., Westra, S. and Sharma, A. (2010) Observed relationships between extreme sub-daily precipitation, surface temperature, and relative humidity. *Geophysical Research Letters*, **37**, L22805.

1153 Hobley, D.E., Sinclair, H.D., and Mudd, S.M. (2012) Reconstruction of a major storm event
1154 from its geomorphic signature: The Ladakh floods, 6 August 2010. *Geology*, **40**, 483-6.

1155 Hooke, R.L. (1967). Processes on arid-region alluvial fans. *The Journal of Geology*, **75**, 438-
1156 460.

1157 Hubert, J.F. and Filipov, A.J. (1989) Debris-flow deposits in alluvial fans on the west flank of
1158 the White Mountains, Owens Valley, California, U.S.A. *Sedimentary Geology*, **61**, 177-205.

1159 Humphrey, N.F. and Heller, P.L. (1995) Natural oscillations in coupled geomorphic systems:
1160 An alternative origin for cyclic sedimentation. *Geology,* **23**, 499-502.

1161 Istanbulluoglu, E. & Bras, R.L. (2006) On the dynamics of soil moisture, vegetation, and
1162 erosion: Implications of climate variability and change. *Water Resources Research*, **42**,
1163 W06418.

1164 Iverson, R.M. (1997) The physics of debris flows. *Reviews of Geophysics*, **35**, 245-296.

1165 Iverson, R.M., Logan, M., LaHusen, R.G. & Berti, M. (2010) The perfect debris flow?
1166 Aggregated results from 28 large-scale experiments. *Journal of Geophysical Research*, **115**,
1167 F03005.

1168 Jayko A.S. (2009) Deformation of the late Miocene to Pliocene Inyo Surface, eastern Sierra
1169 Region, California. In: Oldow J.S. & Cashman P.H. (Eds) *Late Cenozoic structure and*
1170 *evolution of the Great Basin-Sierra Nevada transition*, Special Paper **447**. Geological Society
1171 of America: Boulder, CO; 313-350.

1172 Jerolmack, D.J. & Paola, C. (2010) Shredding of environmental signals by sediment transport.
1173 *Geophysical Research Letters*, **37**, L19401.

1174 Johnson, C.G., Kokelaar, B.P., Iverson, R.M., Logan, M., LaHusen, R.G. & Gray, J.M.N.T.
1175 (2012) Grain-size segregation and levee formation in geophysical mass flows. *Journal of*
1176 *Geophysical Research*, **117**, F01032.

1177 Jones, C.H., Farmer, G.L. & Unruh, J. (2004) Tectonics of Pliocene removal of lithosphere of
1178 the Sierra Nevada, California. *Geological Society of America Bulletin*, **116**, 1408-1422.

1179 Kattelmann, R. (1992) Historical floods in the eastern Sierra Nevada. In: Hall, C.A., Doyle-
1180 Jones, V. and Widawski, B. (Eds) *The History of Water in the eastern Sierra Nevada, Owens*
1181 *Valley and White Mountains*. University of California Press, Los Angeles, California, pp. 74-
1182 86.

1183 Kean, J.W., McCoy, S.W., Tucker, G.E., Staley, D.M. & Coe, J.A. (2013) Runoff-generated
1184 debris flows: Observations and modeling of surge initiation, magnitude and frequency. *Journal*
1185 *of Geophysical Research: Earth Surface*, **118**, 2190-2207.3

1186 Kean, J.W., Staley, D.M. & Cannon, S.H. (2011) In situ measurements of post-fire debris flows
1187 in southern California: Comparisons of the timing and magnitude of 24 debris-flow events with
1188 rainfall and soil moisture conditions. *Journal of Geophysical Research*, **116**, F04019.

1189 Kessler, M.A., Anderson, R.S. & Stock, G.M. (2006) Modeling topographic and climatic control
1190 of east-west asymmetry in Sierra Nevada glacier length during the Last Glacial Maximum.
1191 *Journal of Geophysical Research,* **111**, F02002.

1192 Kirby, M.E., Zimmerman, S.R.H., Patterson, W.P. & Rivera, J.J. (2012) A 9170-year record of
1193 decadal-to-multi-centennial scale pluvial episodes from the coastal southwest United States:
1194 a role for atmospheric rivers? *Quaternary Science Reviews*, **46**, 57-65.

1195 Langbein, W.B. & Schumm, S.A. (1958) Yield of sediment in relation to mean annual
1196 precipitation. *Transactions, American Geophysical Union*, **39**, 1076-1084.

1197 Lau, N.-C. (1997) Interactions between the global SST anomalies and the midlatitude
1198 atmospheric circulation. *Bulletin of the American Meteorological Society*, **78**, 21-33.

1199 Le, K., Lee, J., Owen, L.A., Finkel, R. (2007) Late Quaternary slip rates along the Sierra
1200 Nevada frontal fault zone, California: Slip partitioning across the western margin of the Eastern
1201 California Shear Zone – Basin and Range Province. *GSA Bulletin*, **119**, 240-256.

1202 Lenderink, G. & Van Meijgaard, E. (2008) Increase in hourly precipitation extremes beyond
1203 expectations from temperature changes. *Nature Geoscience*, **1**, 511-514.

1204 Lenderink, G., Mok, H.Y., Lee, T.C. and Van Oldenborgh, G.J. (2011) Scaling and trends of
1205 hourly precipitation extremes in two different climate zones – Hong Kong and the Netherlands.
1206 *Hydrology and Earth System Sciences*, **15**, 3033-3041.

1207 Lisiecki, L.E. & Raymo, M.E. (2009) Diachronous benthic $\delta^{18}O$ responses during late
1208 Pleistocene terminations. *Paleoceanography*, **24**, PA3210.

1209 Liu, S.C., Fu, C., Shiu, C-J., Chen, J.P. & Wu, F. (2009) Temperature dependence of global
1210 precipitation extremes. *Geophysical Research Letters*, **36**, L17702.

1211 Lyle, M., Heusser, L., Ravelo, C., Andreasen, D., Lyle, A.O. & Diffenbaugh, N. (2010)
1212 Pleistocene water cycle and eastern boundary current processes along the California
1213 continental margin. *Paleoceanography*, **25**, PA4211.

Lyle, M., Heusser, L., Ravelo, C., Yamamoto, M., Barron, J., Diffenbaugh, N.S., Herbert, T. & Andreasen, D. (2012) Out of the tropics: The Pacific, Great Basin lakes, and late Pleistocene water cycle in the western United States. *Science*, 1629-1633.

Martel, S.J., Harrison, T.M. & Gillespie, A.R. (1987) Late Quaternary vertical displacement rate across the Fish Springs fault, Owens Valley fault zone, California. *Quaternary Research*, **27**, 113-129.

McCoy, S.W., Kean, J.W., Coe, J.A., Tucker, G.E., Staley, G.M. & Wasklewicz, T.A. (2012) Sediment entrainment by debris flows: In situ measurements from the headwaters of a steep catchment. *Journal of Geophysical Research*, **117**, F03016.

McCoy, S.W., Tucker, G.E., Kean, J.W. & Coe, J.A. (2013) Field measurement of basal forces generated by erosive debris flows. *Journal of Geophysical Research: Earth Surface*, **118**, 589-602.

McDonald, E., McFadden, L.D. & Wells, S.G. (2003) Regional response of alluvial fans to the Pleistocene-Holocene climatic transition, Mojave Desert, California. In: Enzel, Y., Wells, S.G. & Lancaster, N. (Eds) *Paleoenvironments and paleohydrology of the Mojave and southern Great Basin Deserts*, Special Paper 368. Geological Society of America: Boulder, CO; pp. 189-205.

McPhillips, D., Bierman, PR., Crocker, T. & Rood, DH. (2013) Landscape response to Pleistocene-Holocene precipitation change in the Western Cordillera, Peru: ^{10}Be concentrations in modern sediments and terrace fills. *Journal of Geophysical Research: Earth Surface*, **118**, 2488-2499.

Menking, K.M. (1997) Climatic signals in clay mineralogy and grain-size variations in Owens Lake core OL-92. southeast California. In: Smith, G.I. & Bischoff, J.L. (Eds) *An 800,000-year paleoclimatic record from core OL-92, Owens Lake, southeast California*, Special Paper 317. Geological Society of America: Boulder, CO; pp. 25-36.

Menking, K.M., Anderson, R.Y., Shafike, N.G., Syed, K.H. & Allen, B.D. (2004) Wetter or colder at the Last Glacial Maximum? Revisiting the pluvial lake question in southwestern North America. *Quaternary Research*, **62**, 280-288.

Miller, D.M., Schmidt, K.M., Mahan, S.A., McGeehin, J.P., Owen, L.A., Barron, J.A., Lehmkuhl, F. and Löhrer, R. (2010) Holocene landscape response to seasonality of storms in the Mojave Desert. *Quaternary International*, **215**, 45-61.

Molnar, P. & England, P. (1990) Late Cenozoic uplift of mountain ranges and global climate change: chicken or egg? *Nature*, **346**, 29-34.

1247 Moore, J.G. & Mack, G.S. (2008) *Map Showing Limits of Tahoe Glaciation in Sequoia and*
1248 *Kings Canyon National Parks, California*. Scientific Investigations Map 2945, U.S. Geological
1249 Survey (1:125,000).

1250 Moore, J.G. & Sisson, T.W. (1987) *Preliminary geologic map of Sequoia and Kings Canyon*
1251 *National Parks*. Open File Report 87-651, U.S. Geological Survey (1:125,000).

1252 Moore, J.G. (1981) *Geologic map of the Mount Whitney quadrangle, Inyo and Tulare Counties,*
1253 *California*. Geologic Quadrangle Map GQ-1545, U.S. Geological Survey (1:62,500).

1254 NOAA National Climatic Data Center (2014), 2004–2013 climate records from Independence
1255 station. Climate Data Online: www.ncdc.noaa.gov/cdo-web/datasets (accessed 07/10/2014).

1256 Orme, A.R. & Orme, A.J. (2008) Late Pleistocene shorelines of Owens Lake, California, and
1257 their hydroclimatic and tectonic implications. In: In: Reheis, M.C., Hershler, R. and Miller, D.M
1258 (Eds) *Late Cenozoic drainage history of the southwestern Great Basin and lower Colorado*
1259 *River region: Geologic and biologic perspectives*. Geological Society of America Special
1260 Paper 439, Boulder, CO, USA, pp. 207-225.

1261 Oster, J.L., Ibarra, D.E., Winnick, M.J. & Maher, K. (2015) Steering of westerly storms over
1262 western North America at the Last Glacial Maximum. *Nature Geoscience*, **8**, 201-205.

1263 Owen, L.A., Clemmens, S.J., Finkel, R.C. & Gray, H. (2014) Late Quaternary alluvial fans at
1264 the eastern end of the San Bernardino Mountains, Southern California. *Quaternary Science*
1265 *Reviews*, **87**, 114-134.

1266 Pakiser, L.C., Kane, M.F. & Jackson, W.H. (1964) Structural geology and volcanism of Owens
1267 Valley region, California - a geophysical study. Professional Paper 438, U.S. Geological
1268 Survey, pp. 68.

1269 Paola, C. & Foufoula-Georgiou (2001) *Statistical geometry and dynamics of braided rivers*. In:
1270 Mosley, M. P. (Ed) Gravel-Bed Rivers. New Zealand Hydrological Society, Wellington, pp. 47-
1271 71.

1272 Paola, C. (2000) Quantitative models of sedimentary basin filling. *Sedimentology*, **47**, 121-
1273 178.

1274 Paola, C., Heller, P.L. & Angevine, C.L. (1992) The large-scale dynamics of grain-size
1275 variation in alluvial basins, 1: Theory. *Basin Research*, **4**, 73-90.

1276 Paola, C., Straub, K., Mohrig, D. & Reinhardt, L. (2009) The “unreasonable effectiveness” of
1277 stratigraphic and geomorphic experiments. *Earth-Science Reviews*, **97**, 1-43.

Pelletier, J.D. (2014) The linkages among hillslope-vegetation changes, elevation, and the timing of late-Quaternary fluvial-system aggradation in the Mojave Desert revisited. *Earth Surface Dynamics*, **2**, 455-468.

Persson, P.O.G., Neiman, P.J., Walter, B., Bao, J-W. & Ralph, F.M. (2005) Contributions from California coastal-zone surface fluxes to heavy coastal precipitation: A CALJET case study during the strong El Niño of 1998. *Monthly Weather Review*, **133**, 1175-1198.

Phillips, F.M. (2008) Geological and hydrological history of the paleo-Owens River drainage since the late Miocene. In: Reheis, M.C., Hershler, R. & Miller, D.M (Eds) *Late Cenozoic drainage history of the southwestern Great Basin and lower Colorado River region: Geologic and biologic perspectives*. Geological Society of America Special Paper 439, Boulder, CO, USA, pp. 115-150.

Phillips, F.M., Zreda, M., Plummer, M.A., Elmore, D. & Clark, D.H. (2009) Glacial geology and chronology of Bishop Creek and vicinity, eastern Sierra Nevada, California. *Geological Society of America Bulletin*, **121**, 1013-1033.

PRISM Climate Group (2004), Oregon State University: http://prism.oregonstate.edu/ (created 04/02/2004).

Quade, J., Forester, R.M. & Whelan, J.F. (2003) Late Quaternary paleohydrologic and paleotemperature change in southern Nevada. In: In: Enzel, Y., Wells, S.G. & Lancaster, N. (Eds) *Paleoenvironments and paleohydrology of the Mojave and southern Great Basin Deserts*, Special Paper 368. Geological Society of America: Boulder, CO; pp. 165-189.

Rengers, F.K., McGuire, L.A., Kean, J.W., Staley, D.M. & Hobley D.E.J. (2016) Model simulations of flood and debris flow timing in steep catchments after wildfire. *Water Resources Research*, **52**, 6041-6061.

Riebe, C.S., Sklar, L.S., Lukens, C.E. & Shuster, D.L. (2015) Climate and topography control the size and flux of sediment produced on steep mountain slopes. *Proceedings of the National Academy of Sciences*, **112**, 15574-15579.

Rohais, S., Bonnet, S. & Eschard, R. (2012) Sedimentary record of tectonic and climatic erosional perturbations in an experimental coupled catchment-fan system. *Basin Research,* **24**, 198-212.

Rood, D.H., Burbank, D.W. & Finkel, R.C. (2011) Chronology of glaciations in the Sierra Nevada, California, from ^{10}Be surface exposure dating. *Quaternary Science Reviews*, **30**, 646-661.

1310 Schildgen, T.F., Robinson, R.A.J., Savi, S., Phillips, W.M., Spencer, J.Q.G., Bookhagen, B.,
1311 Scherler, D., Tofelde, S., Alonso, R.N., Kubik, P.W., Binnie, S.A. and Strecker, M.R. (2016)
1312 Landscape response to late Pleistocene climate change in NW Argentina: Sediment flux
1313 modulated by basin geometry and connectivity. *Journal of Geophysical Research: Earth*
1314 *Surface*, **121**, 392-414.

1315 Shaw, S.B., Royem, A.A. & Riha, S.J. (2011) The relationship between extreme hourly
1316 precipitation and surface temperature in different hydroclimatic regions of the United States.
1317 *Journal of Hydrometeorology*, **12**, 319-325.

1318 Simpson, G. & Castelltort, S. (2012) Model shows that rivers transmit high-frequency climate
1319 cycles to the sedimentary record. *Geology,* **40**, 1131-1134.

1320 Singleton, A. & Toumi, R. (2013) Super-Clausius-Clapeyron scaling of rainfall in a model squall
1321 line. *Quarterly Journal of the Royal Meteorological Society*, **139**, 334-339.

1322 Sklar, L.S., Riebe, C.S., Marshall, J.A., Genetti, J., Leclere, S., Lukens, C.L. and Merces, V.
1323 (2016) The problem of predicting the size distribution of sediment supplied by hillslopes to
1324 rivers. *Geomorphology*, in press, doi:10.1016/j.geomorph.2016.05.005.

1325 Spelz, R.M., Fletcher, J.M., Owen, L.A. & Caffee, M.W. (2008) Quaternary alluvial-fan
1326 development, climate and morphologic dating of fault scarps in Laguna Salada, Baja
1327 California, Mexico. *Geomorphology*, **102**, 578-594.

1328 Staley, D.M., Wasklewicz, T.A. & Kean, J.W. (2014) Characterizing the primary material
1329 sources and dominant erosional processes for post-fire debris-flow initiation in a headwater
1330 basin using multi-temporal terrestrial laser scanning data. *Geomorphology*, **214**, 324-338.

1331 Steffen, D., Schlunegger, F. & Preusser, F. (2009) Drainage basin response to climate change
1332 in the Pisco valley, Peru. *Geology,* **37**, 491-494.

1333 Steffen, D., Schlunegger, F. & Preusser, F. (2010) Late Pleistocene fans and terraces in the
1334 Majes valley, southern Peru, and their relation to climatic variations. *International Journal of*
1335 *Earth Sciences,* **99**, 1975-1989.

1336 Stock, G.M., Anderson, R.S. & Finkel, R.C. (2004) Pace of landscape evolution in the Sierra
1337 Nevada, California, revealed by cosmogenic dating of cave sediments. *Geology*, **32**, 193-196.

1338 Stock, G.M., Ehlers, T.A. & Farley, K.A. (2006) Where does sediment come from? Quantifying
1339 catchment erosion with detrital apatite (U-Th)/He thermochronometry. *Geology*, **34**, 725-728.

1340 Stock, J.D. & Dietrich, W.E. (2006) Erosion of steepland valleys by debris flows. *Geological*
1341 *Society of America Bulletin*, **118**, 1125-1148.

1342 Stock, J.D., Schmidt, K.M. & Miller, D.M. (2007) Controls on alluvial fan long profiles.
1343 *Geological Society of America Bulletin*, **120**, 619-640.

1344 Thompson, R.S., Anderson, K.H. & Bartlein, P.J. (1999) *Quantitative paleoclimatic*
1345 *reconstructions from late Pleistocene plant macrofossils of the Yucca Mountain region*. U.S.
1346 Geological Survey Open-File Report 99-338, pp. 39.

1347 Torres Acosta, V., Schildgen, T.F., Clarke, B.A., Scherler, D., Bookhagen, B., Wittmann, H.,
1348 Ouimet, W., von Blanckenburg, F. and Strecker, M.R., (2015). The effect of vegetation cover
1349 on millennial-scale landscape denudation in East Africa. *Lithosphere*, **7**, 408-420.

1350 Trenberth, K.E. (2011) Changes in precipitation with climate change. *Climate Research*, **47**,
1351 123-138.

1352 Trenberth, K.E., Dai, A., Rasmussen, R.M. & Parsons, D.B. (2003) The changing character of
1353 precipitation. *Bulletin of the American Meteorological Society*, **84**, 1205-1217.

1354 Trenberth, K.E., Fasullo, J. and Smith, L. (2005) Trends and variability in column-integrated
1355 water vapor. *Climate Dynamics*, **24**, 741-758.

1356 Tucker, G.E. & Slingerland, R. (1997) Drainage basin responses to climate change. *Water*
1357 *Resources Research*, **33**, 2031-2047.

1358 Utsumi, N., Seto, S., Kanae, S., Maeda, E.E. and Oki, T. (2011) Does higher surface
1359 temperature intensify extreme precipitation? *Geophysical Research Letters*, **38**, L16708.

1360 Wakabayashi, J. & Sawyer, T.L. (2001) Stream incision, tectonics, uplift, and evolution of
1361 topography of the Sierra Nevada, California. *The Journal of Geology*, **109**, 539-562.

1362 Waters, J.V., Jones, S.J. & Armstrong, H.A. (2010) Climatic controls on late Pleistocene
1363 alluvial fans, Cyprus. *Geomorphology,* **115**, 228-251.

1364 Wentz, F.J., Ricciardulli, L., Hilburn, K. & Mears, C. (2007) How much more rain will global
1365 warming bring? *Science*, **317**, 233-235.

1366 Whipple, K.X. & Dunne, T. (1992) The influence of debris-flow rheology on fan morphology,
1367 Owens Valley, California. *GSA Bulletin*, **104**, 887-900.

1368 Whittaker, A.C. (2012) How do landscapes record tectonics and climate? *Lithosphere,* **4**, 160-
1369 164.

1370 Whittaker, A.C., Attal, M. & Allen, P.A. (2010) Characterising the origin, nature and fate of
1371 sediment exported from catchments perturbed by active tectonics. *Basin Research*, **22**, 809-
1372 828.

1373 Whittaker, A.C., Cowie, P.A., Attal, M., Tucker, G.E. & Roberts, G.P. (2007) Contrasting
1374 transient and steady-state rivers crossing active normal faults: new field observations from the
1375 Central Apennines, Italy. *Basin Research*, **19**, 529-556.

1376 Winograd, I.J., Landwehr, J.M., Coplen, T.B., Sharp, W.D., Riggs, A.C., Ludwig, K.R. &
1377 Kolesar, P.T. (2006) Devils Hole, Nevada, $\delta^{18}O$ record extended to the mid-Holocene.
1378 *Quaternary Research*, **66**, 202-212.

1379 Winograd, I.J., Landwehr, J.M., Ludwig, K.R., Coplen, T.B. & Riggs, A.C. (1997) Duration and
1380 structure of the past four interglaciations. *Quaternary Research*, **48**, 141-154.

1381 Wolman, M.G. (1954) A method of sampling coarse river bed material. *Transactions, American*
1382 *Geophysical Union,* **35**, 951-956.

1383 Woolfenden, W.B. (2003) A 180,000-year pollen record from Owens Lake, CA: Terrestrial
1384 vegetation change on orbital scales. *Quaternary Research*, **59**, 430-444.

1385 Yamamoto, M., Yamamuro, M. & Tanaka, Y. (2007) The California current system during the
1386 last 136,000 years: Response of the North Pacific High to precessional forcing. *Quaternary*
1387 *Science Reviews*, **26**, 405-414.

1388 Zehfuss, P.H., Bierman, P.R., Gillespie, A.R., Burke, R.M. & Caffee, M.W. (2001) Slip rates
1389 on the Fish Springs fault, Owens Valley, California, deduced from cosmogenic ^{10}Be and ^{26}Al
1390 and soil development on fan surfaces. *Geological Society of America Bulletin*, **113**, 241–255.

10. Figures

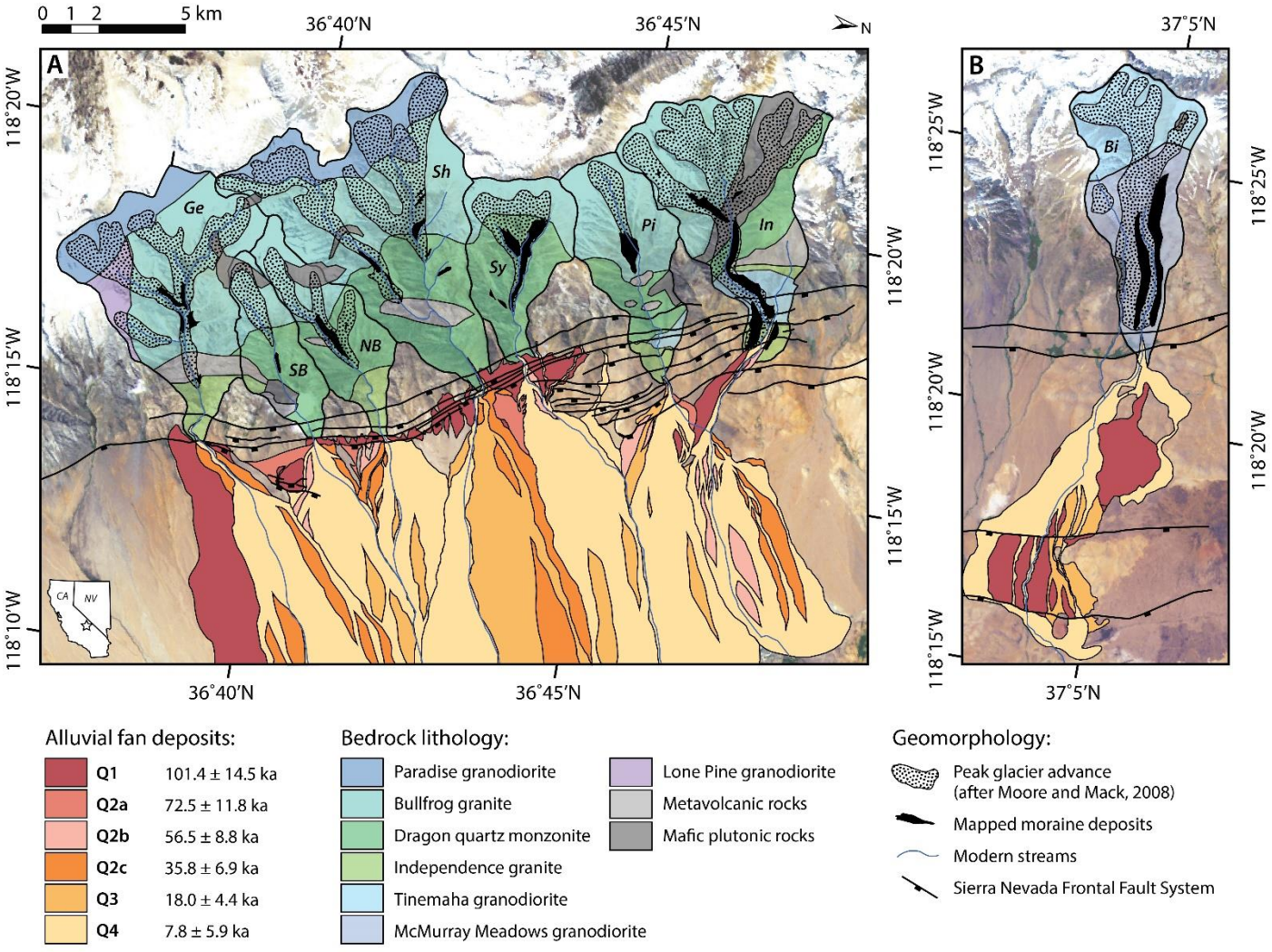
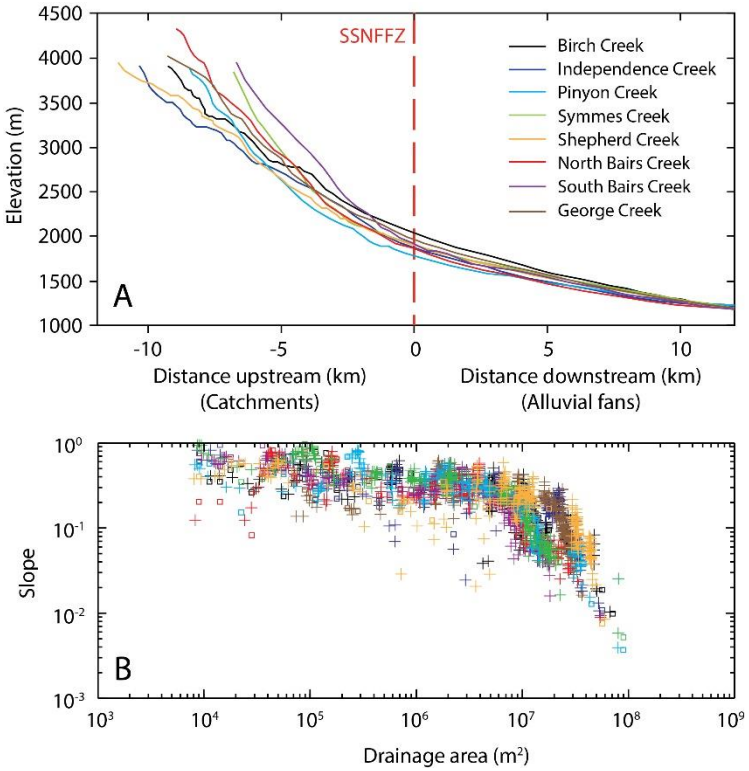


Fig. 1. Maps locating the targeted catchment-fan systems draining from the Sierra Nevada to Owens Valley, California. **(A)** From south to north, these are the George Creek (Ge, 24.8 km^2), South Bairs Creek (SB, 8.0 km^2), North Bairs Creek (NB, 10.1 km^2), Shepherd Creek (Sh, 33.9 km^2), Symmes Creek (Sy, 11.8 km^2), Pinyon Creek (Pi, 13 km^2), and Independence Creek (In, 25.6 km^2) systems. **(B)** We also sampled the Birch Creek (Bi, 17.9 km^2) system, which is located ~40 km north in Owens Valley. Alluvial fan surfaces were mapped following D'Arcy et al. (2015). All catchments are eroding granitic bedrock apart from minor outcrops of metavolcanic and mafic plutonic rocks (Moore, 1981; Moore and Sisson, 1987). The maximum extent of past glaciation is shown by dotted shapes after Moore and Mack (2008); some catchments were fully glaciated in the past (e.g., Independence and Birch Creeks), while others were only partially glaciated (e.g., South Bairs and Pinyon Creeks). Today the catchments are unglaciated apart from very small rock glaciers in north-facing cirques.



407

408

409 **Fig. 2. (A)** Longitudinal profiles for the 8 catchment-fan systems studied. The catchments are steep and
410 erode ~2000 m of relief, independent of channel length. Those that experienced the most glaciation have
411 stepped profiles, e.g., Birch and Independence Creeks, punctuated by hanging valleys. The alluvial fans are
412 ~10 km long and form a coalesced bajada with surface slopes of 4 to 6 °. *SSNFFZ* = Southern Sierra Nevada
413 Frontal Fault Zone. **(B)** Log slope-area plots for all 8 catchments, which show the same longitudinal geometry
414 characteristic of debris flow-scoured landscapes (Stock and Dietrich, 2006).

415



Fig. 3. Representative field photographs. **(A)** Hillslopes at the top of Independence Creek catchment. **(B)** Main valley at the bottom of Independence Creek catchment, viewing upstream. The U-shaped trough is evidence of former glaciation, and the road is cut into moraine deposits with embedded boulders visible in the right-foreground. **(C)** The apex of Shepherd Creek fan, viewing towards the catchment. Abandoned fan surfaces are distinctly visible, incised by younger deposits. The modern debris flow channel is down-cutting into Holocene deposits and is marked by the tops of trees. In the background, the lower parts of the catchment are more densely vegetated than at the top of the catchments shown in (A). **(D)** The terminal nose of a Holocene debris flow deposit on the Shepherd Creek fan. Note the person on the nose for scale. There is a segregation of grain size between boulder-rich levees and finer, gravel-rich channels. **(E)** Cross-sectional view of a debris flow levee, looking across the channel perpendicular to the flow direction. There is an inverse

grading of grain size, with larger boulders and cobbles rafted to the top of the deposit. **(F)** The trunk channel in the Symmes Creek catchment (1 km upstream of the fan apex) after a debris flow in 2013.

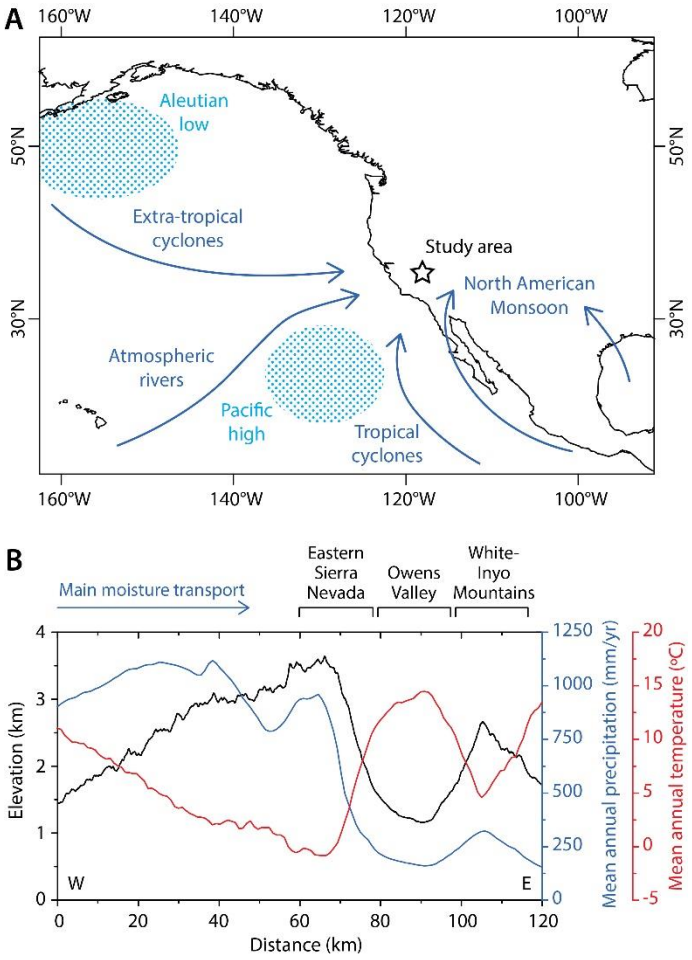


Fig. 4. (A) Schematic map of the main moisture sources affecting our study area in the SW United States (c.f., Antinao and McDonald, 2013a). These are extra-tropical cyclones, 'pineapple express' storms delivered by atmospheric rivers, the remnants of tropical cyclones originating in the eastern Pacific, and moisture transported from the south by the North American Monsoon. The Aleutian low and Pacific high are shown for reference. **(B)** 80 km wide west-to-east swath taken across the Sierra Nevada at 36.8 °S (centred on our study catchments), showing topographic relief (black), and mean annual precipitation (blue) and temperature (red) (PRISM climate group, 2004). As the dominant moisture transport is from the west, Owens Valley occupies a significant orographic rain shadow.

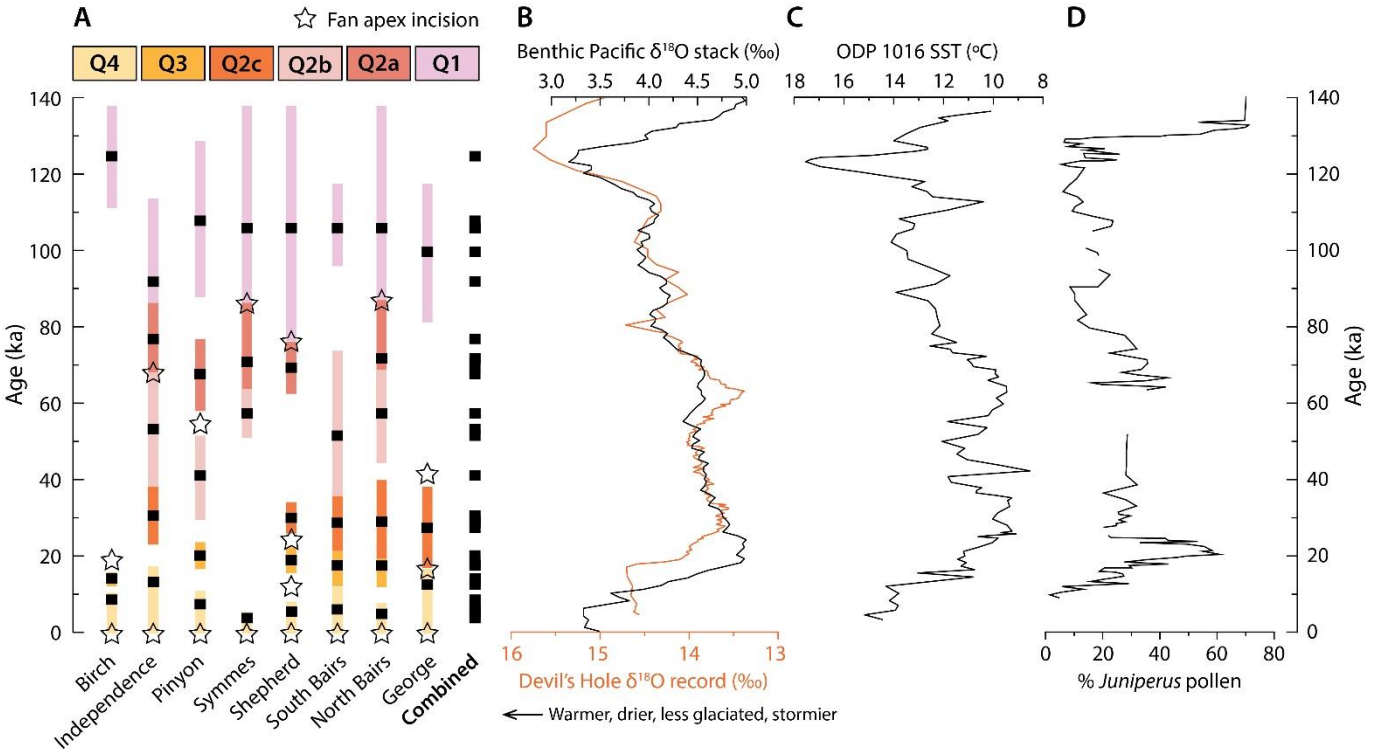


Fig. 5. (A) Stratigraphy and exposure ages for the 8 target fan systems, following D'Arcy et al. (2015) and based on ^{10}Be cosmogenic nuclide exposure dating by Zehfuss et al. (2001), Dühnforth et al. (2007), and Le et al. (2007). Surfaces correspond to the maps in Fig. 1, with black squares showing the best age estimate and coloured bars showing uncertainty. Stars show the timing of incision events at the fan apices. The combined record to the right collapses all mean exposure ages into a single record; this study area offers a high density of age constraints throughout the last glacial-interglacial cycle. **(B)** Two oxygen isotope records are shown for comparison: the benthic $\delta^{18}O$ stack for the Pacific ocean reported by Lisiecki and Raymo (2009) (black) and the terrestrial Devil's Hole $\delta^{18}O$ record from southern Nevada (Winograd et al., 1997; 2006). **(C)** Alkenone-derived sea surface temperature reconstruction from the ODP-1016 core in the Santa Barbara basin, offshore California (Yamamoto et al., 2007). This is the closest sea surface temperature record to our study area and shows fluctuations from ~10° C at the glacial maximum to ~16°C in the interglacials. **(D)** A semi-continuous *Juniperus* pollen record from Owens Lake core OL-92 in Owens Valley (Woolfenden, 2003). Higher *Juniperus* abundances correspond with cooler glacial conditions when juniper woodland expanded to lower elevations that are today covered by desert shrub assemblages.

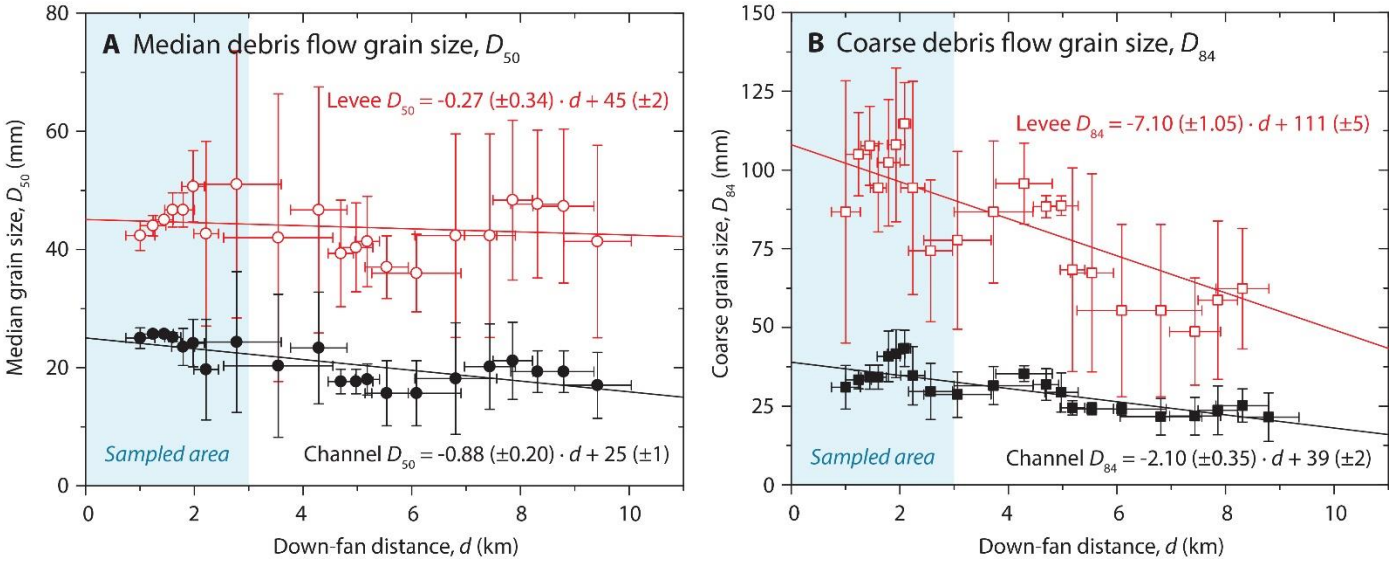


Fig. 6. Debris flow grain size data from the Q4 (Holocene) surface of the Shepherd Creek fan, from apex to toe. Median, D_{50} **(A)**, and coarse, D_{84} **(B)** percentiles are shown. Each point is a spatial average of 3 Wolman point count measurements, and channels and levees were sampled separately. Error bars show the spatial spread of each 3 localities down-system and the variability in grain size between them. Repeat sampling is essential for a meaningful average, as the flow deposits are variable across space (see text for discussion). Down-system fining can be modelled with linear regressions, with average fining rates of 0.3 to 0.9 mm km^{-1} for D_{50} and 2 to 7 mm km^{-1} for D_{84}. To minimise these effects, all other grain size data in this study were collected from the upper 3 km of the fans near their apices (blue box).

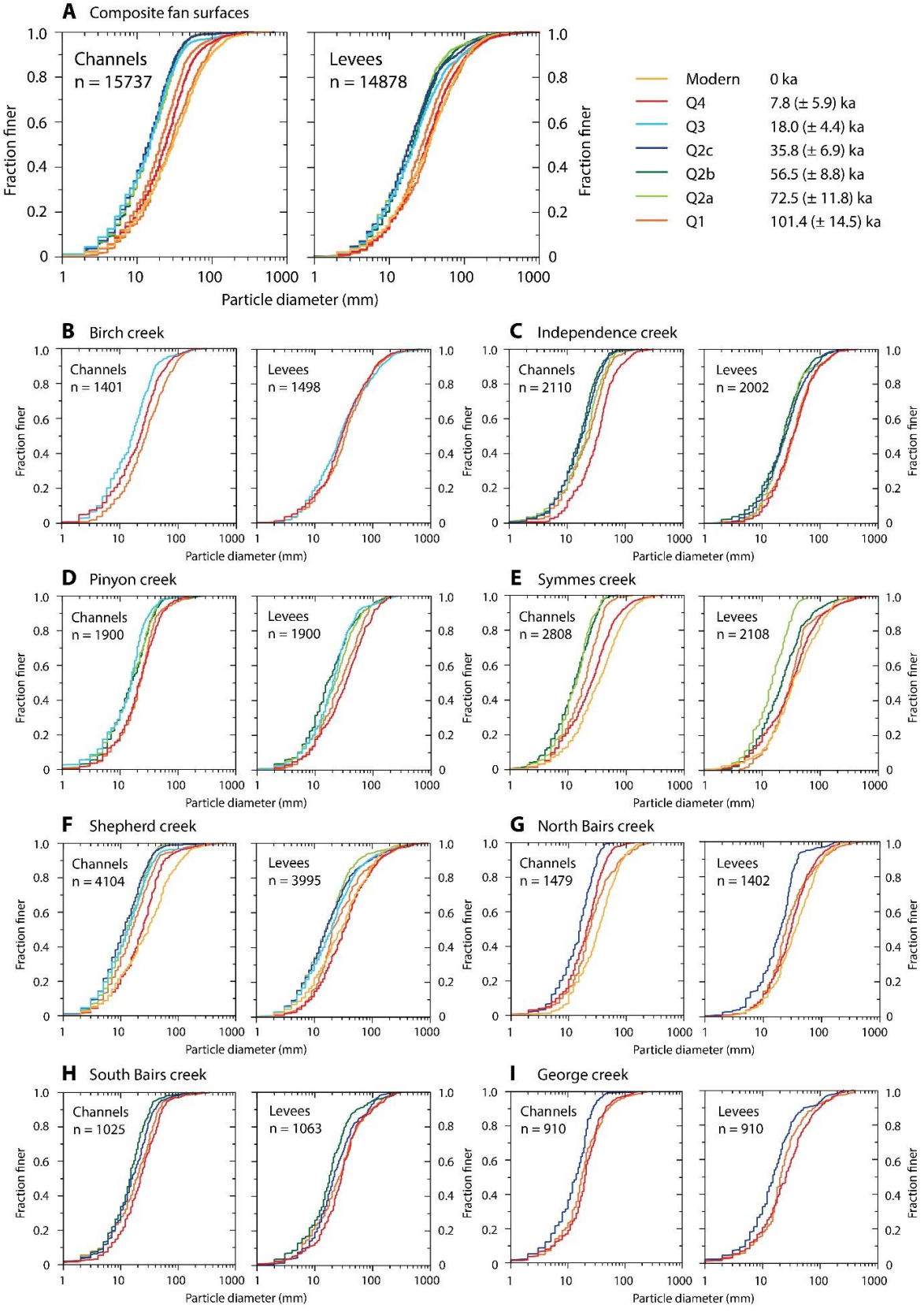


Fig. 7. Cumulative grain size distribution curves for the fan surfaces, with channels on the left and levees on the right. **(A)** Composite of all data from all 8 fans. **(B to I)** Individual fan systems. The number of grains measured is given as *n* and curves are coloured according to stratigraphic unit, with cool colours representing more glacial conditions and warmer colours representing more interglacial conditions. Deposits from interglacial periods are measurably coarser-grained across 3 orders of magnitude in particle size.

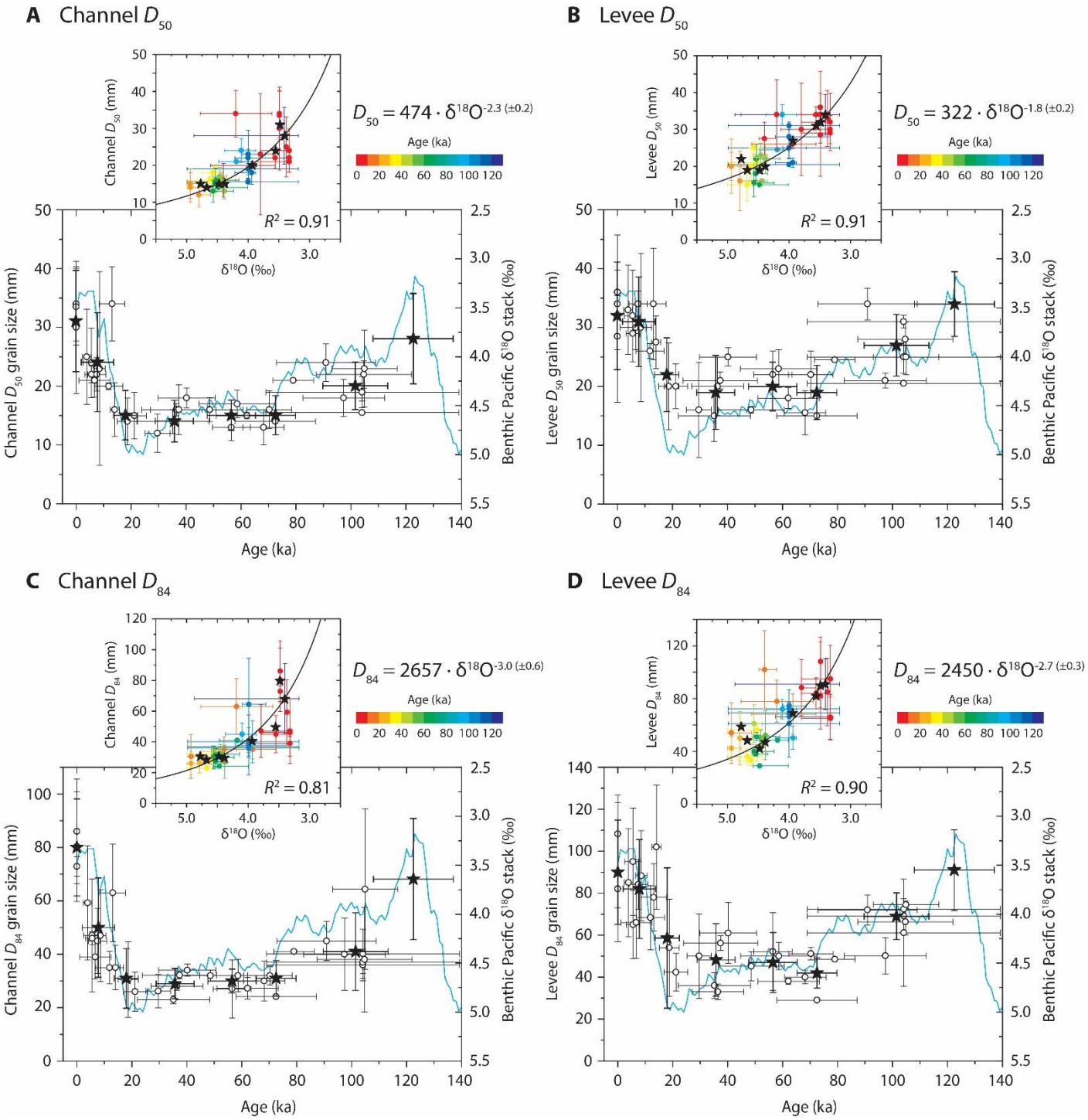
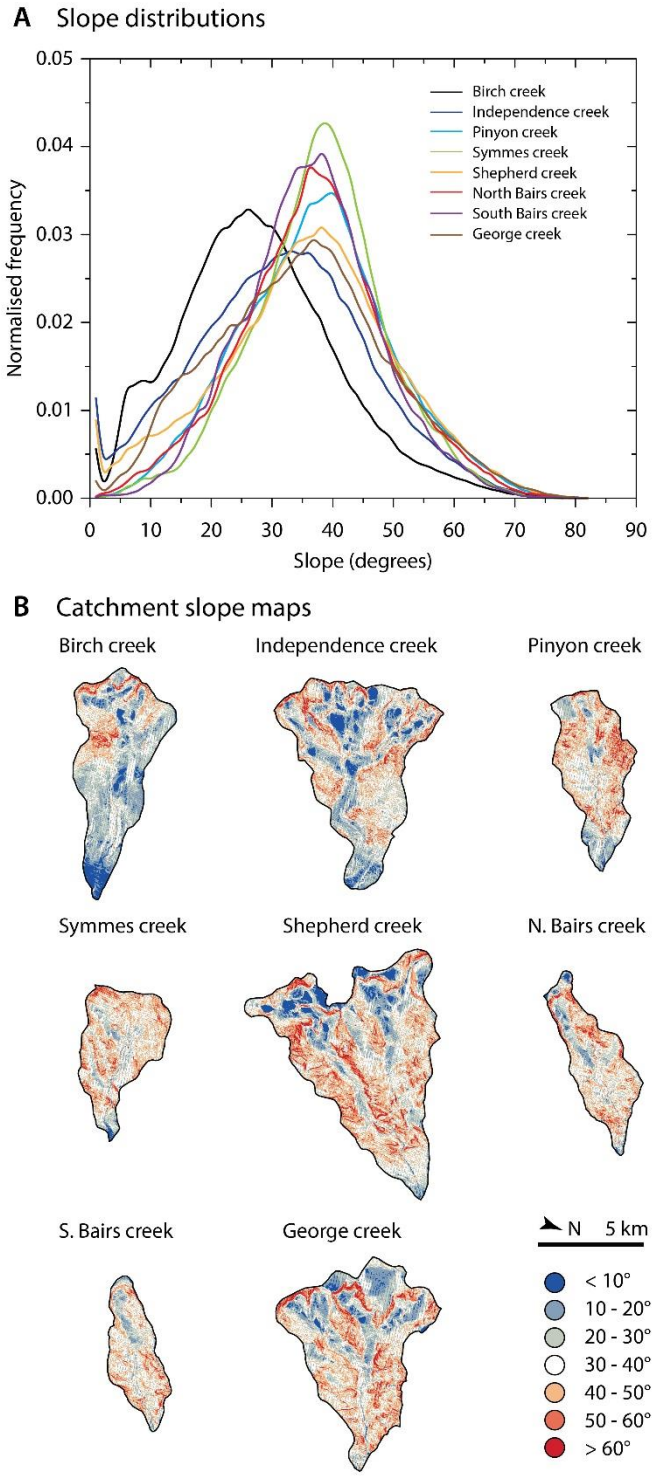


Fig. 8. Grain size percentiles (D_{50}, top; D_{84}, bottom) plotted against fan surface age for debris flow channels (left) and levees (right). Individual fan surfaces are plotted as open circles, stratigraphic averages are plotted as black stars. Error bars show the total age uncertainty and ±1 standard deviation on grain size. The benthic Pacific $\delta^{18}O$ stack of Lisiecki and Raymo (2009) is shown in blue as an illustration of past climate. In all four data series there is a sustained correlation between grain size and climate, with finer grain sizes deposited during glacial periods and coarser grain sizes deposited during interglacial periods. Inset panels show grain size plotted directly against the $\delta^{18}O$ record. Individual fan surfaces are coloured according to their ages, and power law regressions are fitted to the stratigraphic averages (black stars).



482

483 **Fig. 9.** Catchment slope analysis. **(A)** Frequency distributions of slopes in each catchment (the area under
484 each curve is normalised to 1), measured using the National Elevation Dataset with a horizontal/vertical
485 resolution of 9.0/1.5 m. **(B)** Maps of surface slope for each catchment. Formerly glaciated troughs are clearly
486 visible as zones of low slope, and are typically surrounded by steep slopes of ≥50 °.

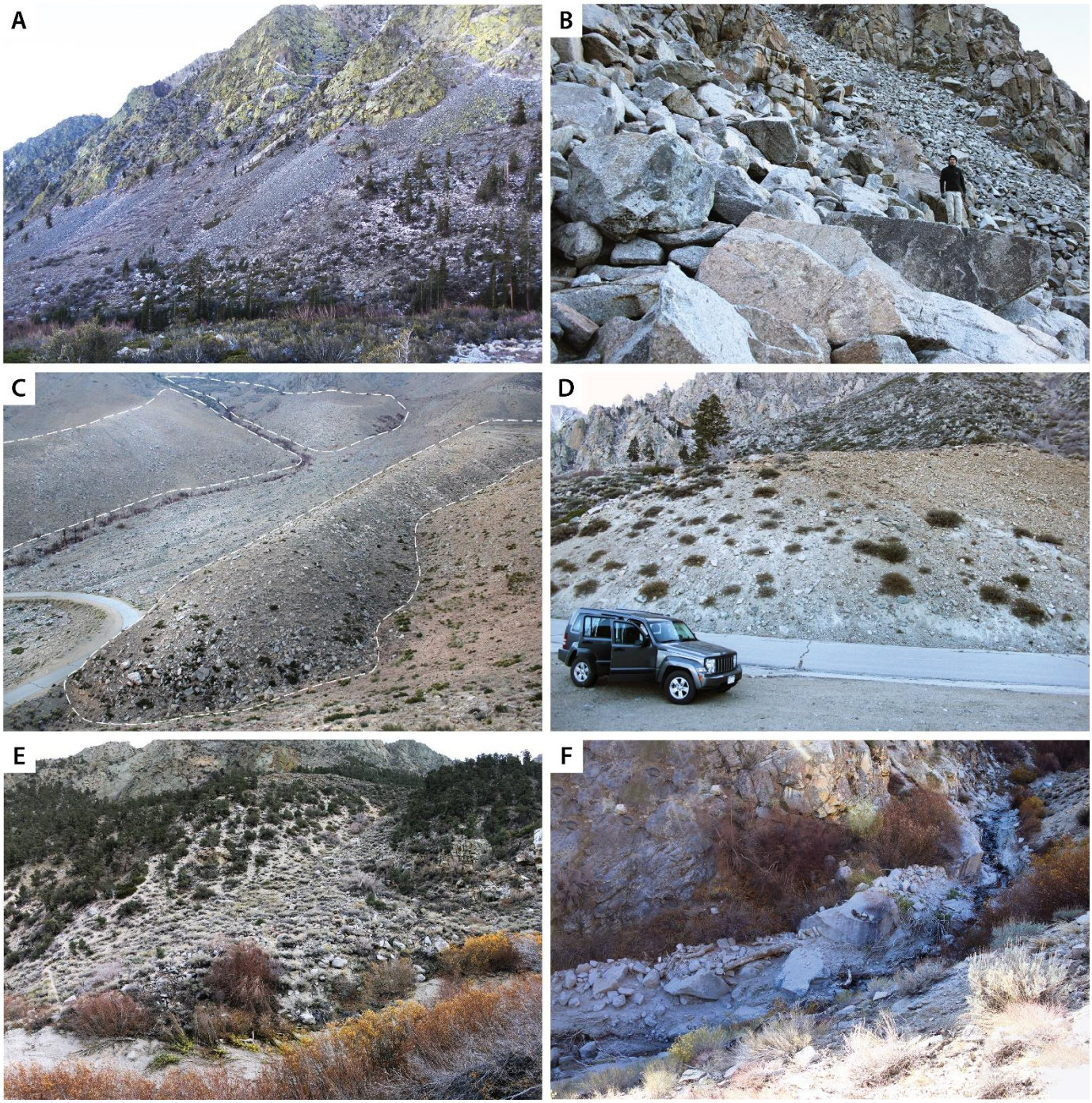


Fig. 10. Field photographs of the main sediment sources. **(A)** Scree cones eroded from the Dragon pluton in the Independence Creek catchment. **(B)** Detail of scree cones in the Independence Creek catchment; note the man for scale. **(C)** Lateral moraines (white dashed outline) at the mouth of the Independence Creek catchment (see Fig. 1). The active channel is marked by trees and sits in a 210 m-wide Q4 fan surface with numerous debris flow levees visible. **(D)** Detail of a road cut through a moraine in the Independence Creek catchment, comprising an unsorted mass of boulders, cobbles, gravel and finer sediment. **(E)** A landslide in the Symmes Creek catchment, toe-cut by the active debris flow channel. Note how the larger boulders sit at the base of the landslide. **(F)** A confined section of the Symmes Creek catchment where debris flows are scouring bedrock directly. Note the large boulders and tree trunk debris rafted to the inner levee of the flow bend.

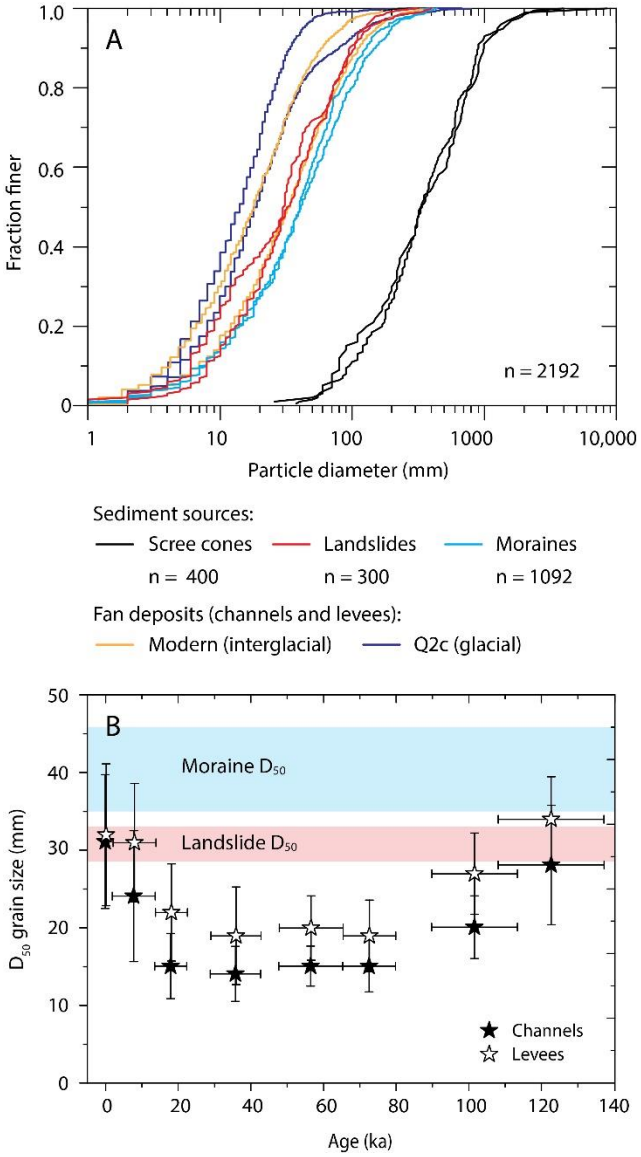


Fig. 11. (A) Cumulative grain size distribution curves for the main sediment sources in the catchments: scree cones (black), landslides (red) and moraine deposits (blue). These were sampled in the Symmes Creek and Independence Creek catchments, which are not distinguished because the grain size distributions are so similar in each case. A total of 2192 grain size counts were made from sediment sources. For comparison, modern (yellow) and Q2c (dark blue) grain size data are shown for the debris flow deposits in Fig. 7. The coarser curves are levees and the finer curves are channels. **(B)** A comparison of moraine D_{50} (blue box) and landslide D_{50} (red box) with the average D_{50} grain sizes for debris flow channels (black stars) and levees (white stars) in Fig. 8. The coloured boxes show D_{50} ±1 standard deviation. Moraine deposits supply sediment that is ~10 mm coarser than landslides on average. Both sediment sources lie at the coarsest end-member of the fan deposits sampled.

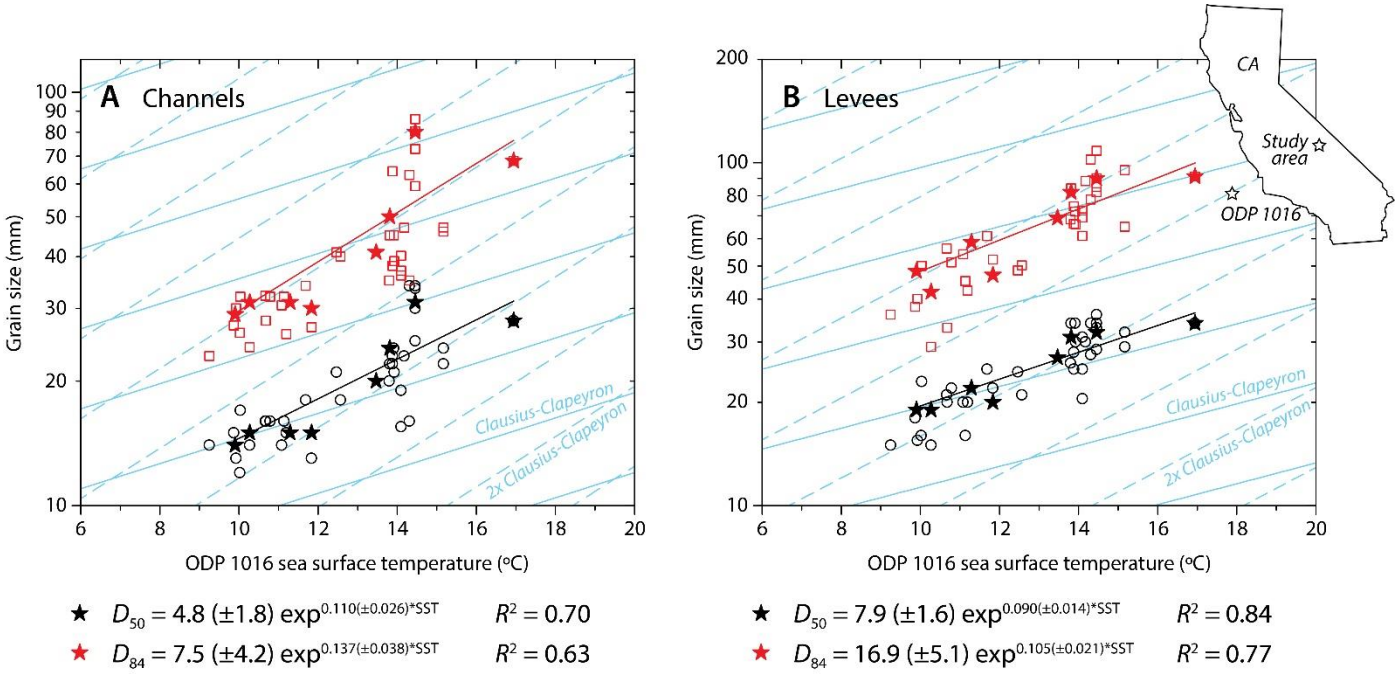
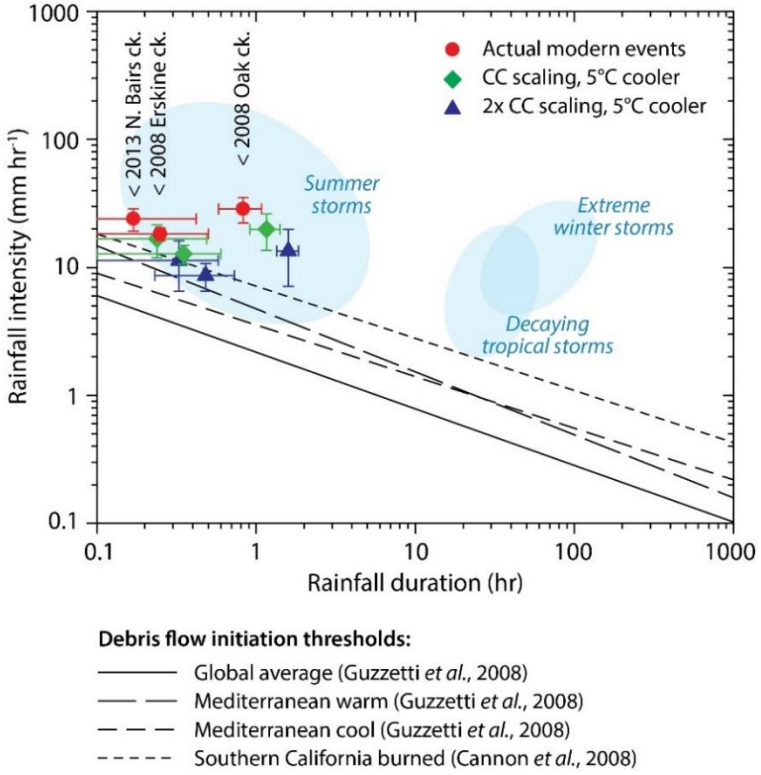


Fig. 12. Grain size percentiles (D_{50}, black; D_{84}; red) from Fig. 8 plotted against the ODP-1016 sea surface temperature record of Yamamoto et al. (2007) for **(A)** debris flow channels and **(B)** debris flow levees. Open symbols show individual fan surfaces and stars show stratigraphic averages, which are fitted with exponential regressions (quoted beneath the graphs). The *y*-axes are logged because the relationships are non-linear. Blue lines in the background show the Clausius-Clapeyron (CC, solid lines) and 2 x CC (dashed lines) scalings, which describe how storm rainfall intensity varies as a function of temperature (see text for details and references). In all four series, grain size coarsens at an intermediate rate (between 9.0 and 13.7 % per 1 °C) for the full ~6 °C temperature range captured by the last glacial-interglacial cycle.



530

531

532 **Fig. 13.** Rainfall intensity-duration thresholds for debris flow initiation, including the global average and for
533 Mediterranean climates (Guzzetti et al., 2008) and burned landscapes in southern California (Cannon et al.,
534 2008). The main moisture sources affecting our study area today are highlighted in blue after Antinao and
535 McDonald (2013a). Three examples of modern storms that initiated debris flows in our study area are shown
536 in red after DeGraff et al. (2011); all were summer thunderstorms. For each event, we then hypothetically
537 scale down rainfall intensity by the Clausius-Clapeyron (green) and 2x Clausius-Clapeyron (blue)
538 relationships (see text for details) for a temperature decrease of 5 °C. This does not move storm events below
539 the debris flow initiation thresholds, i.e., debris flows could still be initiated under an LGM-style temperature
540 scenario if storm intensity changes with temperature following our expectations.

11. Tables

Alluvial fan	Surface	Age (ka)	± (ka)	Debris flow channels					Debris flow levees				
				No. clasts	D_{50} (mm)	± (mm)	D_{84} (mm)	± (mm)	No. clasts	D_{50} (mm)	± (mm)	D_{84} (mm)	± (mm)
Symmes creek	Modern	-	-	497	34.0	6.3	86.0	19.7	210	34.0	1.4	108.2	18.6
Shepherd creek	Modern	-	-	699	30.0	11.2	80.3	20.6	500	28.5	11.2	90.0	33.2
North Bairs creek	Modern	-	-	302	33.5	6.5	72.8	3.7	300	36.0	9.8	82.0	8.9
Symmes creek	Q4	3.9	1.6	1212	25.0	8.1	59.2	21.3	1098	33.0	7.6	85.0	25.8
Shepherd creek	Q4	5.5	3.0	1007	24.0	5.9	47.0	21.2	1195	32.0	7.8	95.0	25.6
South Bairs creek	Q4	5.6	2.4	213	22.0	1.4	46.0	2.4	210	29.0	-	65.0	16.2
North Bairs creek	Q4	6.7	5.7	674	21.0	2.9	39.0	8.1	600	30.0	3.8	66.0	17.0
Pinyon creek	Q4	7.5	3.4	400	22.0	2.8	45.0	12.2	400	34.0	2.2	84.2	11.8
Birch creek	Q4	8.5	2.1	501	23.0	16.5	47.0	17.2	500	30.0	12.6	88.3	21.4
George creek	Q4	11.9	5.1	300	20.0	0.6	35.0	6.1	300	26.0	1.3	68.3	15.2
Independence creek	Q4	13.1	4.6	610	34.0	6.3	63.0	18.2	501	34.0	9.5	78.0	16.0
Birch creek	Q3	14.1	1.7	500	16.0	4.5	35.0	8.3	598	27.5	4.5	102.0	29.5
Shepherd creek	Q3	18.7	3.7	998	14.0	4.0	30.5	14.2	999	20.0	7.3	54.0	23.1
Pinyon creek	Q3	21.2	4.3	600	15.0	4.0	26.0	7.3	600	20.0	3.8	42.3	9.0
Shepherd creek	Q2c	29.6	4.5	900	12.0	3.3	26.2	6.3	801	16.0	8.1	50.0	20.1
George creek	Q2c	35.2	13.2	310	14.0	2.0	23.0	1.6	310	15.0	4.4	36.0	6.1
North Bairs creek	Q2c	36.4	9.4	200	16.0	1.1	28.0	1.4	200	20.0	4.9	33.0	3.8
South Bairs creek	Q2c	37.4	13.5	200	16.0	4.2	32.2	1.4	250	21.0	1.4	56.2	3.5
Independence creek	Q2c	40.2	10.4	400	18.0	1.7	34.0	2.3	401	25.0	1.6	61.0	14.4
Pinyon creek	Q2b	48.6	12.0	300	16.0	2.0	32.0	2.0	300	16.0	0.6	45.2	7.0
Symmes creek	Q2b	56.5	6.9	699	13.0	2.2	27.0	10.9	500	22.0	4.0	52.2	18.5
Independence creek	Q2b	58.6	13.9	500	17.0	2.4	32.0	6.1	500	23.0	3.2	50.0	6.5
South Bairs creek	Q2b	62.1	11.2	312	15.0	0.6	27.2	4.0	303	18.0	1.8	38.0	1.6
Shepherd creek	Q2a	68.2	7.5	300	13.0	3.0	30.0	7.4	400	15.5	3.8	40.0	3.2
Pinyon creek	Q2a	70.3	8.1	300	16.0	3.2	32.0	3.5	300	22.0	4.0	51.2	3.0
Symmes creek	Q2a	72.5	14.6	100	14.0	-	24.2	-	100	15.0	-	29.0	-
Independence creek	Q2a	79.0	7.4	100	21.0	-	41.0	-	100	24.5	-	48.5	-
Independence creek	Q1	90.9	18.1	500	24.0	3.2	45.0	7.3	500	34.0	2.7	72.0	7.2
George creek	Q1	97.4	14.9	300	18.0	3.1	40.0	13.5	300	21.0	1.3	50.2	8.7
Symmes creek	Q1	104.1	35.1	300	19.0	2.6	36.0	5.9	200	31.0	1.1	61.1	25.5
Shepherd creek	Q1	104.1	35.1	200	15.5	-	37.0	4.2	100	20.5	-	72.4	-
South Bairs creek	Q1	104.1	35.1	300	19.0	1.5	40.2	9.2	300	25.0	2.8	69.2	8.2
Pinyon creek	Q1	104.7	17.3	300	22.0	2.3	38.0	19.5	300	28.0	2.9	66.3	6.1
North Bairs creek	Q1	104.9	11.9	303	23.0	6.5	64.4	30.0	302	25.0	3.0	74.5	1.8
Birch creek	Q1	122.5	14.5	400	28.0	7.7	68.2	22.7	400	34.0	5.5	91.0	19.3

Table 1. Grain size data measured on individual fan surfaces by Wolman point counting in the field, in the upper 3 km of each fan system. Surface ages are reported after D'Arcy et al. (2015). The error on grain size measurements reflects ±1 standard deviation of D_{50} or D_{84} if it is calculated for each single sampling locality, and therefore reflects spatial variability.

Alluvial fan	Surface	Age (ka)	± (ka)	Debris flow channels					Debris flow levees				
				No. clasts	D_{50} (mm)	± (mm)	D_{84} (mm)	± (mm)	No. clasts	D_{50} (mm)	± (mm)	D_{84} (mm)	± (mm)
All fans	Modern	-	-	1498	31.0	8.6	80.0	18.1	1010	32.0	9.1	90.0	24.9
All fans	Q4	7.8	5.9	4917	24.0	8.4	50.0	18.6	4804	31.0	7.6	82.0	23.5
All fans	Q3	18.0	4.4	2098	15.0	4.2	31.0	11.2	2197	22.0	6.3	58.6	33.4
All fans	Q2c	35.8	6.9	2010	14.0	3.5	29.0	5.7	1962	19.0	6.3	48.2	17.3
All fans	Q2b	56.5	8.8	1811	15.0	2.6	30.0	4.5	1603	20.0	4.1	47.0	14.3
All fans	Q2a	72.5	7.3	800	15.0	3.3	31.0	6.7	900	19.0	4.6	42.0	7.2
All fans	Q1	101.4	11.8	2203	20.0	4.0	41.0	14.5	2002	27.0	5.2	69.0	11.1
Birch creek	Q1	122.5	14.5	400	28.0	7.7	68.2	22.7	400	34.0	5.5	91.0	19.3

Table 2. Grain size data compiled for each stratigraphic unit, using data from all 8 fan systems sampled in the field (given in Table 1). The Q1 surface on the Birch Creek fan is separated from the other Q1 surfaces because it is significantly older by about 20 ka and is interpreted to date to the last interglacial period (see Methods and D'Arcy et al., 2015). Grain size percentiles are measured from the total grain size data set for each stratigraphic unit (they are not averages of the D_{50} and D_{84} values quoted in Table 1). The error on grain size measurements reflects ±1 standard deviation of D_{50} or D_{84} if it is calculated for each single sampling locality, and therefore reflects spatial variability.

Sediment source	No. clasts	D_{50} (mm)	± (mm)	D_{84} (mm)	± (mm)
Independence creek					
Moraines	692	41.0	4.5	113.0	6.0
Scree	200	340.0	84.0	820.0	15.3
Landslides	200	33.0	-	82.0	18.3
Symmes creek					
Moraines	400	40.0	5.1	100.0	26.4
Scree	200	335.0	-	900.0	-
Landslides	100	30.5	1.8	85.0	10.8

Table 3. Grain size measurements for major sediment sources sampled in the Independence and Symmes Creek catchments. Both catchments show remarkably similar grain size properties for moraines, scree cones and landslides, which is attributed to the uniform granitic lithology in this study area.